

## Review

## Evolution of light use efficiency models: Improvement, uncertainties, and implications



Yanyan Pei<sup>a</sup>, Jinwei Dong<sup>a,\*</sup>, Yao Zhang<sup>b</sup>, Wenping Yuan<sup>c</sup>, Russell Doughty<sup>d</sup>, Jilin Yang<sup>a</sup>, Decheng Zhou<sup>f</sup>, Liangxia Zhang<sup>f</sup>, Xiangming Xiao<sup>e,\*</sup>

<sup>a</sup> Key Laboratory of Land Surface Pattern and Simulation, Institute of Geographic Sciences and Natural Resources Research, Chinese Academy of Sciences, Beijing 100101, China

<sup>b</sup> Sino-French Institute for Earth System Science, College of Urban and Environmental Sciences, Peking University, Beijing, China

<sup>c</sup> School of Atmospheric Sciences, Guangdong Province Key Laboratory for Climate Change and Natural Disaster Studies, Sun Yat-sen University, Zhuhai, Guangdong 510245, China

<sup>d</sup> College of Atmospheric and Geographic Sciences, GeoCarb Mission, University of Oklahoma, Norman, OK, 73072, USA;

<sup>e</sup> Department of Microbiology and Plant Biology, Center for Earth Observation and Modeling, University of Oklahoma, Norman, OK 73019, USA

<sup>f</sup> Jiangsu Key Laboratory of Agricultural Meteorology, Nanjing University of Information Science and Technology, Nanjing 210044, China

## ARTICLE INFO

## Keywords:

Gross primary production (GPP)  
Light use efficiency (LUE)  
Photochemical reflectance index (PRI)  
Solar-induced fluorescence (SIF)  
Complexity  
Simplicity

## ABSTRACT

Light use efficiency (LUE) models have been widely used to estimate terrestrial gross primary production (GPP) at local, regional, and global scales, which is vital for understanding the carbon flux dynamics under climate change. LUE models express GPP as the product of the incoming photosynthetically active radiation (PAR), the fraction of PAR absorbed by plants (FPAR), the maximum LUE, and the environmental stress factors (e.g., temperature, water, and carbon dioxide). Here, we investigate 21 LUE models reported in literatures and conclude their complicated evolutions in the aforementioned four components: 1) the representation of PAR was improved from total PAR to direct and diffuse PARs; 2) the representation of FPAR was improved from one-leaf to two-leaf (i.e., sunlit and shaded leaves) or chlorophyll based strategies; 3) the parameterization of the maximum LUE was improved from a constant value of 0.39 gC/MJ to the C3/C4- and sunlit/shaded leaf-specific values; and 4) the representation of environmental stress factors was improved both in their integration forms (e.g., from the multiplication method to the law of the minimum method) and the proxy optimization for a specific stress factor. For example, the proxy for water stress factor has evolved from atmospheric (e.g., vapor pressure deficit) and soil (e.g., soil moisture) water indicators to the plant (e.g., land surface water index) water indicators. We also identify uncertainties caused by model structures, parameterizations, input data with various resolutions and accuracies, and scale mismatch issues between remote sensing data and flux tower observations. The newly emerged indicators such as the photochemical reflectance index, solar-induced chlorophyll fluorescence, and near-infrared reflectance of vegetation simplify the methods to estimate GPP but fail to disentangle the influences of different environmental factors. These findings on the evolution of LUE models and their uncertainties are expected to contribute to future model improvements.

## 1. Introduction

Gross primary production (GPP) is defined as the total amount of carbon dioxide ( $\text{CO}_2$ ) fixed by plants over a period (e.g., hour, day, year) through photosynthesis (Beer et al. 2010; Ryu et al. 2019; Stocker et al. 2019; Zhang et al. 2020). As the largest  $\text{CO}_2$  flux in the global carbon cycle, terrestrial GPP plays an important role in the seasonal dynamics and inter-annual variation of atmospheric  $\text{CO}_2$  concentration. It also has

been considered as a key indicator of ecological goods and services for the society, such as food, fiber, and energy (He et al. 2013; Yuan et al. 2007). Thus, the estimation of terrestrial GPP is an indispensable prerequisite for understanding the carbon cycle, climate change, and ecosystem services (Anav et al. 2015; Beer et al. 2010; He et al. 2013; Jiang and Ryu 2016; Le Quere et al. 2016; Xia et al. 2015; Yuan et al. 2014; Zhang et al. 2019b; Zhang et al. 2017; Zhao et al. 2005).

The GPP estimation is difficult as no direct measures are available at

\* Corresponding author.

E-mail addresses: [dongjw@igsnrr.ac.cn](mailto:dongjw@igsnrr.ac.cn) (J. Dong), [xiangming.xiao@ou.edu](mailto:xiangming.xiao@ou.edu) (X. Xiao).

scales larger than the leaf level (Welp et al. 2011). Net ecosystem exchange (NEE) of CO<sub>2</sub> between the land surface and the atmosphere data from the eddy covariance (EC) flux tower sites can be used to indirectly estimate GPP at the canopy level, and have been widely used as reference data for calibrating and validating GPP models (Baldocchi 2014; Baldocchi et al. 2001; Jiang and Ryu 2016; Jung et al. 2020; Wang et al. 2017; Zhang et al. 2017). However, at the regional and global scales, the estimation of terrestrial GPP relies largely upon various types of models (Yuan et al. 2007).

Generally, the existing GPP models can be classified as statistical, process-based, and light use efficiency (LUE) models (Zhang et al. 2016c). The statistical models are based on the relationships between in situ carbon flux observations and remote sensing/climate variables, such as the near-infrared reflectance of terrestrial vegetation (NIR<sub>V</sub>), the canopy structure-related NIR<sub>V</sub> multiplied by incoming sunlight (NIR<sub>V</sub>P), and the kernel normalized difference vegetation index (kNDVI) (Badgley et al. 2017b; Camps-Valls et al. 2021; Dechant et al. 2022). Statistical models are valuable for their applicability to represent the effects of climate change or variability directly, but they usually lack a rigorous theoretical basis of physiological ecology (Sun and Zhu 1999). Also, the accuracy of the statistical models depends largely on the number and representativeness of sites, and the derived empirical relationships have poor generalizability. The process-based models focus on ecological and physiological processes of plant growth, such as the Breathing Earth System Simulator (BESS) (Jiang and Ryu 2016; Ryu et al. 2011) and the Penman-Monteith-Leuning (PML) models (Zhang et al. 2019b). However, this kind of models usually need a large set of input data and parameters, some of which are difficult to obtain or are obtainable but have limited accuracy (Zhang et al. 2016b; Zheng et al. 2018).

The LUE models estimate GPP as the energy absorbed by plants multiplied by the actual LUE that converts energy to carbon fixed during the photosynthesis process (Monteith 1972). The LUE-based GPP models such as the Moderate Resolution Imaging Spectroradiometer (MODIS) GPP product (MOD17) (Zhao et al. 2005) and the Vegetation Photosynthesis Model (VPM) (Xiao et al. 2004a; Xiao et al. 2004b), are mainly driven by satellite data. The remote sensing data are characterized by their large spatial coverage, consistency, repeatability, and low cost, and they have the potential to illuminate the spatial and temporal dynamics of plant growth at the regional and global scales (Dong et al. 2015; Hilker et al. 2008; Moreno et al. 2012; Turner et al. 2003; Wu et al. 2012; Wu et al. 2010; Xiao et al. 2004a; Yuan et al. 2019; Zhao et al. 2005). In recent decades, many LUE-based GPP models have been proposed.

However, it is unclear how much the LUE-based GPP models have advanced since the establishment of light use efficiency theory and how each component of the LUE-based GPP model has evolved. A previous study has reviewed the capacity of remote sensing for providing the critical input variables for LUE models (Hilker et al. 2008). We extend this review by conducting a review on the evolution and uncertainties of the 21 most widely used LUE models. The objectives of this review were to 1) investigate the trends in the evolution of these LUE-based GPP models from the perspectives of each model component, 2) understand the uncertainties in different components, and 3) provide insights for further improvements of the models. This review is organized into the following five sections. In Section 2, we introduce the basic theory and structure of LUE-based GPP models. In Section 3, we track the evolution of the 21 LUE-based GPP models. In Section 4, we discuss the uncertainties in LUE models. In Section 5, we highlight the applicability and outlook for improving LUE models. In Section 6, we conclude major findings and implications for global-scale applications.

## 2. Basic theory and structure of LUE GPP models

The LUE models treat GPP as the product of the absorbed photosynthetically active radiation (APAR) and actual LUE (Monteith 1972) and define LUE as the efficiency of the photosystems to use absorbed light energy to fix carbon. It has two fundamental assumptions: (1) GPP

is linearly related to APAR, and (2) the actual LUE ( $\varepsilon_g$ ) is downregulated from its theoretical maximum LUE ( $\varepsilon_0$ ) by environmental conditions, such as temperature or water stress. Note that the CO<sub>2</sub> concentration factor is not a downregulated one. The general form of the LUE-based model can be expressed as:

$$\text{GPP} = \text{APAR} \times \varepsilon_g \quad (1)$$

$$\text{APAR} = \text{PAR} \times \text{FPAR} \quad (2)$$

$$\varepsilon_g = \varepsilon_0 \times f(T, W, \dots) \quad (3)$$

where PAR refers to the photosynthetically active radiation, FPAR is the fraction of PAR that is absorbed, and  $f(T, W, \dots)$  represents environmental conditions, such as air temperature  $f(T_a)$  and soil water  $f(SW)$  (Fig. 1).

## 3. Evolution of LUE GPP models

In this section, we summarized the evolution of LUE models from the perspectives of each model component, including PAR, FPAR, LUE<sub>max</sub>, and environmental stress factors (Fig. 2).

### 3.1. Light sources and amounts: PAR as total, direct, and diffuse PAR

As a fundamental driver for LUE-based GPP models, total PAR has been improved by the division of total PAR into direct and diffuse PAR components. The diffuse radiation is more uniformly distributed in the canopy and penetrates deeper into the canopy, while the direct radiation tends to result in light saturation at the top of the canopy (He et al. 2013). Therefore, the photosynthetic rate under diffuse radiation is more efficient than that under direct radiation. With a given value of total incident radiation, the LUE of the entire canopy will increase as the diffuse radiation fraction ( $f(D_f)$ ) increases. The  $f(D_f)$  has been used to directly estimate actual LUE without any environmental stress factors in the DIFFUSE model (Donohue et al. 2014). Since the proportion of diffuse radiation increase with the cloud cover, the cloudiness index (CI, defined as the difference between 1 and the ratio of PAR to potential PAR) has also been proposed to partition PAR in some GPP models, e.g., CFLUX Model (Turner et al. 2006; Turner et al. 2009), CI-LUE Model (Wang et al. 2015), Coupled Carbon and Water (CCW) Model (Zhang et al. 2016b), Wang's Model (Wang et al. 2018), and CI-Evaporative Fraction (CI-EF) Model (de Almeida et al. 2018).

### 3.2. Light absorption: FPAR by canopy, leaves or chlorophyll

The LUE-based GPP models also evolved in estimating the fraction of absorbed PAR (FPAR) from the PAR absorbed by the canopy (FPAR<sub>canopy</sub>) to the PAR absorbed by sunlit leaves and shade leaves (FPAR<sub>sunlit</sub> and FPAR<sub>shaded</sub>) or the PAR absorbed by chlorophyll (FPAR<sub>chl</sub>) (Xiao et al. 2004a; Xiao et al. 2004b) (Fig. 1).

#### 3.2.1. Light absorption by canopy (FPAR<sub>canopy</sub>)

The original LUE-based GPP models consider the plant canopy as a single big-leaf and use FPAR<sub>canopy</sub> for various plant function types (PFTs) since the 1970s. Different proxies (e.g., Normalized Difference Vegetation Index, NDVI, and Leaf Area Index, LAI) have been used to estimate FPAR<sub>canopy</sub> in LUE models (Prince and Goward 1995; Running et al. 2004). During the late 1990s to the early 2000s, FPAR<sub>canopy</sub> was usually represented by NDVI derived from NOAA/AVHRR or SPOT/VEGETATION, such as the Global Production Efficiency Model (GLO-PEM) (Prince and Goward 1995) and Carbon-Fix (C-Fix) models (Veroustraete et al. 2002). Since the launch of the Terra and Aqua satellites, the MODIS FPAR/LAI, NDVI, and enhanced vegetation index (EVI) products have been commonly used to estimate FPAR<sub>canopy</sub>. For example, the MOD17 (Zhao et al. 2005), Carbon Flux (CFLUX) (Turner et al. 2006), Two

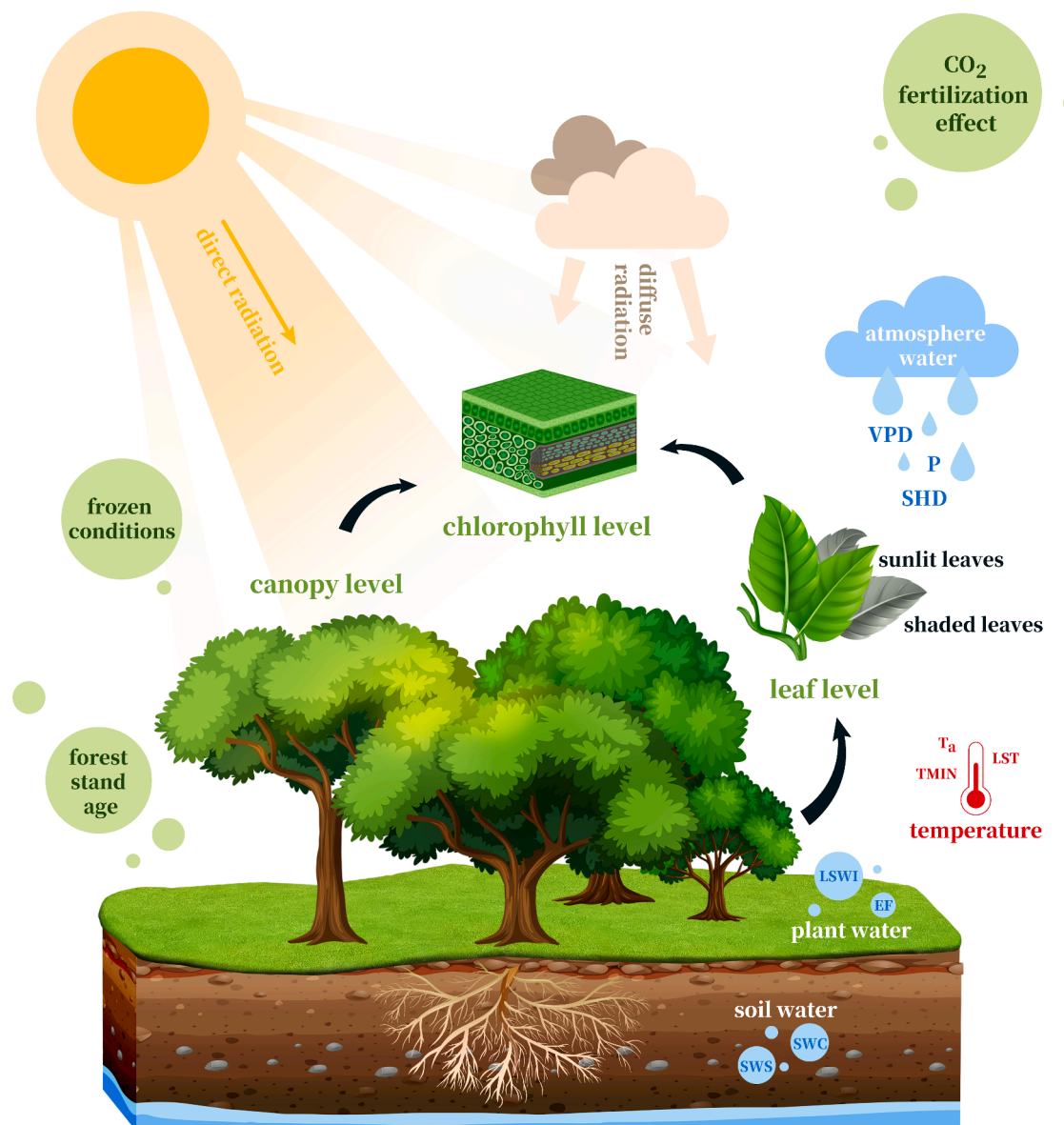


**Fig. 1.** The basic theory of the light use efficiency (LUE) models ( $GPP = PAR \times FPAR \times LUE$ ). PAR includes direct and diffuse radiation, and FPAR in this figure is non-specific in that it can represent FPAR by the canopy, leaves (sunlit and shaded leaves), and/or chlorophyll. LUE is attenuated from its theoretical maximum by environmental conditions, such as air temperature, water, and atmospheric CO<sub>2</sub> concentration. See the acronyms table for all the abbreviations.

Leaf-LUE (TL-LUE) (He et al. 2013), nonlinear TL-LUE (TL-LUEn) (Wu et al. 2015), Terrestrial Ecosystem Carbon Flux Model (TEC) (Yan et al. 2015), CI-LUE, Terrestrial Carbon Flux (TCF) (He et al. 2016), Diffuse Fraction-Based Two-Leaf Light Use Efficiency (DTEC) (Yan et al. 2017a), and CI-EF use the MODIS FPAR (MOD15) product (Table 1). The Eddy-Covariance Light Use Efficiency (EC-LUE) (Yuan et al. 2010; Yuan et al. 2007; Yuan et al. 2019), DIFFUSE, modified Vegetation Photosynthesis Model (MVPM) (Zhang et al. 2015a; Zhang et al. 2019a), CCW, and Wang's model use the MODIS NDVI product (Table 1).

The FPAR data products derived from different proxies and data sources differ and affect GPP estimation Ruimy et al. (1999). and Ruimy et al. (1994) underscored that the linear relationship between FPAR and NDVI is an approximation, which is only valid during the growing stage. Also, NDVI tends to saturate in multi-layer closed canopies because of the quick saturation of the red band (Huete et al. 1997; Lees et al. 2018; Walker et al. 2014). FPAR<sub>canopy</sub> derived from LAI was found to be effective in improving LUE-based GPP models compared to MOD17 GPP products based on MOD15 FPAR, especially for agricultural and grassland ecosystems (Xiao et al. 2016; Zhu et al. 2016). The Multi-source

Data Synergized Quantitative GPP (MuSyQ) Model derives FPAR by using measured LAI (Cui et al. 2016b). Zheng et al. (2018) compared the performances of the four different FPAR proxies (i.e., MOD15 FPAR, NDVI, EVI, and LAI) and found that the FPAR data products based on NDVI, EVI, and LAI performed best in grasslands, forests, and croplands, respectively. They also showed that the proxies from different data sources may differ considerably due to varying data quality, algorithms, and data inputs (Zheng et al. 2018). These together suggest that the selection of FPAR in LUE models should consider the potential effects of different proxies, biomes, and geographical characteristics.

### 3.2.2. Light absorption by leaves ( $FPAR_{sunlit}$ and $FPAR_{shaded}$ )

Canopies are composed of sunlit and shaded leaves, which receive different amounts of direct and diffuse incident solar radiation. Specifically, sunlit and shaded leaves differ in their structural, morpho-anatomical, and physiological traits, as well as in the number, shape, and size of chloroplasts (Doerken and Lepetit 2018; Lichtenhaller et al. 1981). Sunlit leaves are usually smaller and thicker than shaded leaves, and they also show a higher leaf mass per area, stomata density,

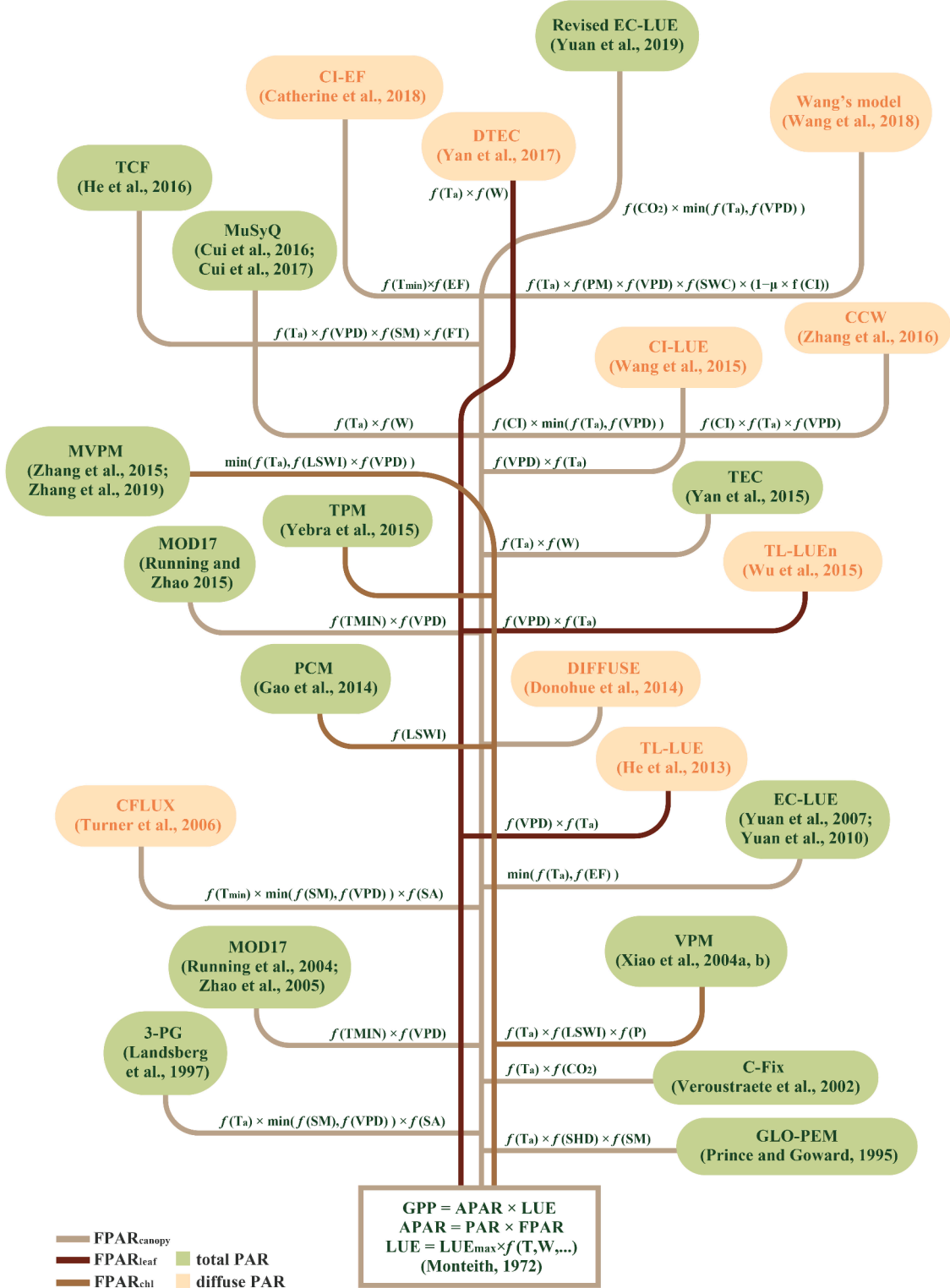


**Fig. 2.** The evolution of LUE GPP models. Rounded rectangles with different colors indicate different PAR levels of the models: the green and orange indicate the models in which total PAR and diffuse PAR are considered, respectively. Lines with different colors indicate different FPAR levels of the models: the light brown, reddish brown, and brown indicate the FPAR at the canopy, leaf (sunlit and shaded), and chlorophyll levels, respectively. The expressions next to the lines indicate the types and integration forms of environmental stress factors for the corresponding models. See the acronyms table for all the abbreviations.

palisade/spongy parenchyma ratio, light saturation rate of photosynthesis, light compensation point, light saturation irradiance, and chlorophyll a/b ratio (Doerken and Lepetit 2018; Lichtenthaler et al. 1981).

As a result, the sunlit and shaded leaves have different photosynthetic rates. Under clear skies, sunlit leaves are often light-saturated.

Their photosynthetic rates are lower and can even decrease with increasing radiation because of enhanced photorespiration (He et al. 2013; Wu et al. 2015). Therefore, the actual LUE of sunlit leaves is relatively lower. On the contrary, shaded leaves are often exposed to diffuse radiation, which is usually much lower than the radiation

**Table 1**

A summary of models that use APAR (and LUE) to estimate daily GPP.

Number	Model Name	Equation	Light reaction		Carbon fixation Maximum LUE or others $\varepsilon_{\max}$	Photosynthesis Regulation Factors			Reference
			Light Absorption (APAR = FPAR × PAR)			PAR	Temperature Scalar (T)	Water Scalar (W)	
			FPAR	PAR	$\varepsilon_{\max}$				
1	GLO-PEM	$GPP=FPAR \times PAR \times \varepsilon_{\max} \times f(T_a) \times f(SHD) \times f(SM)$	$FPAR=1.67 \times NDVI-0.08$	TOMS ultraviolet observations	$f(T_a)=((T-T_{\min})(T-T_{\max}))/((T-T_{\min})(T-T_{\max})-(T-T_{opt})^2)$	$f(SHD)=1-0.05SHD$ ( $0 < SHD \leq 15$ , or 0.25 ( $SHD > 15$ ); $SHD=SSH-SH$ ; $f(SM)=1-\exp(0.081$ ( $SM < 83.3$ ));	$f(SH)=1/(1+(1-(SWC/SWC_{\max})/c)^h)$ $f(VPD)=e^{-k \times VPD}$ ;	$f(SA)=1/(1+(RSA/0.95)^n)$	(Prince and Goward 1995)
2	3-PG	$GPP=FPAR \times PAR \times \varepsilon_{\max} \times f(T_a) \times \min(f(SM), f(VPD)) \times f(SA)$			$f(T_a)=1-FD/TD$	$f(SM)=1/(1+(1-(SWC/SWC_{\max})/c)^h)$ $f(VPD)=e^{-k \times VPD}$ ;	$f(SA)=1/(1+(RSA/0.95)^n)$	(Landsberg and Waring 1997)	
3	MOD17	$GPP=FPAR \times PAR \times \varepsilon_{\max} \times f(TM_{\min}) \times f(VPD)$		NCEP-DOE Reanalysis II (MOD17A2, C5.5)	Look-Up Table	$f(TM_{\min})=1$ ( $TM_{\min} > TM_{\max}$ ), or $(TM_{\max}-TM_{\min})/(TM_{\max}-TM_{\min})$ , $(TM_{\min}-TM_{\min} \leq TM_{\min} \leq TM_{\max})$ , or 0 ( $TM_{\min} < TM_{\min}$ ); or 1 ( $TM_{\min} < TM_{\max}$ );	$f(VPD)=0$ ( $VPD > VPD_{\max}$ , or $(VPD_{\max}-VPD)/(VPD_{\max}-VPD_{\min})$ , $(VPD_{\min} \leq VPD \leq VPD_{\max})$ , or 1 ( $VPD < VPD_{\min}$ );		(Running et al. 2004; Zhao et al. 2005)
4	C-Fix	$GPP=FPAR \times PAR \times \varepsilon_{\max} \times f(T_a) \times f(CO_2)$	$FPAR=0.8642 \times NDVI-0.0814$	World Meteorological Organization (WMO)	1.1 gC/MJ (APAR)	$f(T_a)=e^{(C1-AE/GC \times Ta)/(1+e^{(EN \times Ta-DE)/GC \times Ta})}$		$f(CO_2)=F_{CO_2}/F_{CO_2}^{ref}$	(Veroustraete et al. 2002)
5	VPM	$GPP=FPAR \times PAR \times \varepsilon_{\max} \times f(T_a) \times f(LSWI) \times f(P)$	$FPAR=(EVI-0.1) \times 1.25$	NCEP Reanalysis II	$C3=0.42, C4=0.63$ gC/mol APAR.	$f(T_a)$ is the same as in GLO-PEM.	$f(LSWI)=(1+LSWI)/(1+LSWI_{\max})$		(Xiao et al. 2004a; Xiao et al. 2004b)
6	CFLUX	$GPP=FPAR \times PAR \times \varepsilon_{base} \times f(T_{\min}) \times \min(f(SM), f(VPD)) \times f(SA)$	MODIS FPAR	DAYMET database	$\varepsilon_{base}=(\varepsilon_{\max}-\varepsilon_{cs}) \times f(Cl)+\varepsilon_{cs};$ $f(Cl)=\frac{(Cl_q-Cl_{\min})}{(Cl_{\max}-Cl_{\min})};$ $Cl=1-PAR/\text{PAR}_{po}$	$f(T_{\min})$ is the same as MOD17.	$f(VPD)$ is the same as MOD17.	$f(SA)=GPP/GPP_{\max}$	(King et al. 2011; Turner et al. 2006)
7	EC-LUE	V1: $GPP=FPAR \times PAR \times \varepsilon_{\max} \times \min(f(T_a), f(EF))$ V2: $GPP=FPAR \times PAR \times \varepsilon_{\max} \times \min(f(T_a), f(EF))$ V3: $GPP=FPAR \times PAR \times \varepsilon_{\max} \times f(CO_2) \times \min(f(T_a), f(VPD))$	$FPAR=1.24a \times NDVI-0.168+b$	MERRA archive		$f(T_a)$ is the same as GLO-PEM.	V1: $f(EF)=1/(\beta+1)$ V2: $f(EF)=LE/R_n$ V3: $f(CO_2)=(C_i-0)/(C_i+20)$ , $C_i=C_a \times \chi$ $f(VPD)=VPD_0/(VPD+VPD_0)$		(Yuan et al. 2010; Yuan et al. 2007; Yuan et al. 2019)
8	TL-LUE	$GPP=(\varepsilon_{msu} \times APAR_{sh}=(1-\alpha) \times ((PAR_{dif}-PAR_{dif,u})/LAI+C) \times LAI_{sh};$ $APAR_{su}+e_{msu} \times APAR_{su}=(1-\alpha) \times (PAR_{dif} \times \cos(\lambda)/\cos(\varphi)+$ $APAR_{sh}) \times f(VPD) \times f(T_a)$	$APAR_{dif}=PAR_{dif,u}/LAI+C) \times LAI_{su};$ $LAI_{su}=2 \times \cos(\varphi) \times (1-\exp(-0.5 \times \Omega \times (LAI/\cos(\varphi))))$ $LAI_{sh}=LAI-LAI_{su};$ $PAR_{dif}=PAR \times (0.7527+3.8453SI-16.316SI^2+18.962SI^3-7.0802SI^4);$ $SI=PAR/(0.5 \times S_u \times \cos(\varphi))$	in situ measured PAR	constant value	$f(T_a)$ is the same as MOD17	$f(VPD)$ is the same as MOD17		(He et al. 2013)
9	DIFFUSE	$GPP=FPAR \times PAR \times (0.02D_f+0.00061\varepsilon_{\max})$	MOD13Q1	AWAP climate data	$\varepsilon_{\max} \cdot 12 \mu\text{mol CO}_2 \text{ m}^{-2} \text{ s}^{-1}$			overcast skies: $D_f=1.0$ clear skies: $D_f=0.2$	(Donohue et al. 2014)

(continued on next page)

**Table 1** (continued)

Number	Model Name	Equation	Light reaction		Carbon fixation			Reference
			Light Absorption (APAR = FPAR × PAR)		PAR	Maximum LUE or others	Photosynthesis Regulation Factors	
		FPAR		$\varepsilon_{\max}$	Temperature Scalar (T)	Water Scalar (W)	Other Scalar	
10	PCM	$GPP=PC_{\max} \times f(EVI) \times f(LSWI)$	MODIS		$PC_{\max}=0.1346 \times LST_{an}+2.7522; PC_{\max}: CBS\ 2.61, NM\ 2.06, HBGC\ 1.75, HBSD\ 1.38, DX\ 2.00\ mol\ C\ m^{-2}\ d^{-1}$	$f(LSWI)=(1+LSWI)/(1+LSWI_{\max}); LSWI_{\max}=1$	$f(EVI)=EVI-0.1$	(Gao et al. 2014)
11	TL-LUEn	$GPP=((\varepsilon_m \times APAR_{su} \times \tau)/(\varepsilon_m \times APAR_{su+\tau}) \times LAI_{su}+(\varepsilon_m \times APAR_{sh} \times \tau)/(\varepsilon_m \times APAR_{sh+\tau}) \times LAI_{sh}) \times f(VPD) \times f(T_a)$	MOD15A2 FPAR in situ measured PAR					(Wu et al. 2015)
12	TEC	$GPP=FPAR \times PAR \times \varepsilon_{\max} \times f(T_a) \times f(W)$	MOD15A2 FPAR ECMWF ERA-Interim reanalysis data	C3 1.8, C4 2.76 g	$f(T_a)$ is the same as GLO-PEM. $f(W)=E/E_p$			(Yan et al. 2015)
13	TPM	$GPP=\min(GPP_c, GPP_r); GPP_r=FPAR_{\max}=0.95, GPP_r=FPAR \times PAR \times f(NDVI)=\max(\min((NDVI-0.1)/(0.9-0.1),1),0, \varepsilon_{\max} \times f(EVI))$	FPAR=FPAR <sub>max</sub> × $f(NDVI)$ ; (Sheffield et al. 2006)			$f(EVI)=\max(\min((EVI-0.05)/(0.90-0.05),1),0)$		(Yebra et al. 2015)
14	MVPM	$GPP=FPAR \times PAR \times \varepsilon_{\max} \times \min(f(T_a), f(W))$	MOD09A1 (C6) ChinaFLUX site		$f(T_a)$ is the same as in VPM.	$f(W)=f(LSWI) \times f(VPD); f(LSWI)=(1+LSWI)/(1+LSWI_{\max}) \times P_s; P_s=(1+LSWI)/2$ (before leaf full expansion), or 1 (after leaf full expansion) $f(VPD)=(VPD_{\max}-VPD)/VPD_{\max}$ ( $VPD>0.5\ kPa$ ), or 1 ( $VPD \leq 0.5\ kPa$ )		(Zhang et al. 2015a; Zhang et al. 2019a)
15	CI-LUE	$GPP=FPAR \times PAR \times \varepsilon_{base} \times f(T_a) \times f(VPD)$	MOD15A2 FPAR ChinaFLUX site	$\varepsilon_{base}=(\varepsilon_{\max}-\varepsilon_{cs}) \times f(CI)+\varepsilon_{cs}; f(CI)=(CI_q-Cl_{min})/(Cl_{\max}-Cl_{min}); Cl=1-PAR/PAR_{po}$	$f(T_a)=0\ (T_a \leq T_{\min}),\ or\ (T_a-T_{\min})/(T_{\max}-T_{\min})$ $f(CI)=0\ (VPD \geq VPD_{\max}),\ or\ (VPD_{\max}-VPD)/(VPD_{\max}-VPD_{\min})$ $f(VPD)=(VPD_{\min}<VPD<VPD_{\max}),\ or\ 1\ (VPD \leq VPD_{\min})$			(Wang et al. 2015)
16	MuSyQ	$GPP=FPAR \times PAR \times \varepsilon_{\max} \times f(T_a) \times f(W)$	measured APAR using LI-190SA in situ measured	0.60 gC mol <sup>-1</sup> PPFD	$f(T_a)=T_1 \times T_2; T_1=0.8+0.02T_{opt}-0.005T_{opt}^2; T_2=1.184/((1+e^{0.2(T_{opt}-10-T_a)})(1+e^{0.3(-T_{opt}-10+T_a)}))$	$f(W)=0.5+0.5E/E_p$		(Cui et al. 2016a; Cui et al. 2016b)
17	CCW	$GPP_{or}=FPAR \times PAR \times \varepsilon_{\max} \times f(CI) \times \min(f(T_a), f(VPD)); GPP_{and}=FPAR \times PAR \times \varepsilon_{\max} \times f(CI) \times f(T_a) \times f(VPD)$	MOD13A3 (C5) CRU-NCEP dataset		$f(T_a)$ is the same as GLO-PEM.	$f(VPD)=\exp(-K_2 \times (VPD-VPD_{\min}))$	$f(CI)=1-K_1 \times CI$	(Zhang et al. 2016b)
18	TCF	$GPP=FPAR \times PAR \times \varepsilon_{\max} \times f(T_a) \times f(VPD) \times f(SM) \times f(FT)$	MOD15A2 FPAR MERRA reanalysis			$f(SM)=0\ (SM \leq SM_{\min}),\ or\ (SM-SM_{\min})/(SM_{\max}-SM_{\min})$ $f(FT)=(SM_{\min}<SM<SM_{\max}),\ or\ 1\ (SM \geq SM_{\max})$		(He et al. 2016)

(continued on next page)

Table 1 (continued)

Number	Model Name	Equation	Light reaction Light Absorption (APAR = FPAR × PAR)	PAR	Carbon fixation Maximum LUE or others $\epsilon_{\max}$	Photosynthesis Regulation Factors	Reference
19	DTEC	$GPP = (\epsilon_{\text{msu}} \times APAR_{\text{dh}} - (PAR_{\text{dif}} - PAR_{\text{dif,lu}}) / (LAI + C)) \times LAI_{\text{dh}}$ ; $APAR_{\text{su}} = (PAR_{\text{dif}} \times \cos(\lambda) / \cos(\phi)) + (PAR_{\text{dif}} - PAR_{\text{dif,lu}}) / (LAI + C) \times LAI_{\text{su}}$ ; $LAI_{\text{su}} = 2 \times \cos(\phi) \times (1 - \exp(-0.5 \times \Omega \times (LAI / \cos(\phi))))$ ; $LAI_{\text{dh}} = LAI - LAI_{\text{su}}$ ; $PAR_{\text{dif}} = PAR \times D_f$ ; $D_f = 0.7527 + 3.8453 SI - 16.316 SI^2 + 18.962 SI^3 - 7.0802 SI^4$ ;	FPAR	eddy covariance flux data	$C_3: \epsilon_{\text{msu}} = 3.78 \times D_f^{1.8}, \epsilon_{\text{msu}} = 1.67$ ; $D_f^{1.8}, \epsilon_{\text{msu}} = 5.78 \times D_f^{1.8}, \epsilon_{\text{msu}} = 2.56$ $g \text{ C MJ}^{-1}$ ;	$f(T_a)$ is the same as GLO-PEM. $f(W)$ is the same as TEC	(Van et al. 2017b)
20	Wang et al.; model	$GPP = FPAR \times PAR \times SI - PAR / (0.48 \times S_0 \times \cos(\phi))$ $FPAR = 1.0 \times NDVI - 0.05$	FPAR	eddy covariance flux data	$f(T_a) = 1.184 / ((1 + e^{0.2 \times (T_{\text{opt}} - 10 - T_b)}) (1 + e^{0.3 \times (-T_{\text{opt}} - 10 + T_a)})$ $m^{-2} \text{ MJ}^{-1}$ (without CI/with CI)	$f(SWC) = (SWC - SWC_{\min}) / (SWC_{\max} - SWC_{\min})$ $f(VPD) = 1 / (1 + VPD / D_0)$ , $D_0 = 15 \text{ hPa}$ ;	(Wang et al. 2018)
21	CI-EF	$GPP = FPAR \times PAR \times \epsilon_{\text{base}} \times f(T_{\min}) \times f(EF)$	MOD15A2H FPAR (C6)	eddy covariance flux data	$\epsilon_{\text{base}} = (\epsilon_{\max} - \epsilon_{\text{cs}}) \times f(CI) + \epsilon_{\text{cs}}$ ; $f(CI) = (CI - CI_{\min}) / (CI_{\max} - CI_{\min})$ ; $CI = 1 - PAR_{\text{pos}}$	$f(T_{\min})$ is the same as in MOD17.	(de Almeida et al. 2018)

saturation point. Under cloudy/aerosol-laden skies, incoming radiation is mainly diffuse and therefore the shaded leaves can capture more radiation. Even though the total incident radiation may be lower when the sky is overcast, the increase of diffused radiation by shaded leaves can enhance GPP at the canopy scale.

Based on this theory, He et al. (2013) developed the two-leaf TL-LUE model. The TL-LUE model stratifies the canopy into sunlit and shaded leaves and uses different LUE<sub>max</sub> and APAR values for them (He et al. 2013). Wu et al. (2015) developed the TL-LUEn model to estimate GPP for both sunlit and shaded leaves separately. Using a rectangular hyperbolic function, this model rectified the non-linear relationship between GPP and APAR, which is linear in the TL-LUE model. Other models based on the two-leaf canopy structure include the DTEC model, which improves the calculation of environmental stress factors, especially for water stress (Yan et al. 2017a).

### 3.2.3. Light absorption by chlorophyll (FPAR<sub>chl</sub>)

Another group of studies improved the estimates of FPAR from the biochemical perspective (Xiao et al. 2004a; Xiao et al. 2004b), based on the fact that light absorption by leaf and canopy is composed of two components: (1) light absorbed by chlorophyll (APAR<sub>chl</sub>), which is used for photosynthesis, and (2) light absorbed by the non-photosynthetic vegetation (NPV, APAR<sub>NPV</sub>), which is not involved in photosynthesis. Greenness indices can be used as a proxy of canopy chlorophyll content to estimate GPP (Gitelson et al. 2006). The radiative transfer models were used to estimate light absorption by chlorophyll, leaf and canopy, and the results showed that the seasonal dynamics of EVI agrees well with that of the fraction of light absorbed by chlorophyll (FPAR<sub>chl</sub>) (Zhang et al. 2005; Zhang et al. 2006). EVI can optimize vegetation signals by overcoming the weaknesses in NDVI, including the saturation of NDVI in very dense canopies (Huete et al. 2002; Huete et al. 1997). Thus, some LUE models represent the fraction of PAR absorbed by chlorophyll (FPAR<sub>chl</sub>) as a linear or quadratic function of EVI, including the Vegetation Photosynthesis Model (VPM) (Xiao et al. 2004a; Xiao et al. 2004b), Two-Parameter Model (TPM) (Yebra et al. 2015), and Photosynthetic Capacity Model (PCM) (Gao et al. 2014) (Table 1). Recent advances in leaf chlorophyll content inversions may provide better FPAR<sub>chl</sub> estimates (Croft et al. 2020).

### 3.3. Maximum light use efficiency (LUE<sub>max</sub>): from constant values to biome-, C3/C4-, and sunlit/shaded-specific values

The parameterization of LUE<sub>max</sub> in the LUE-based GPP models can be divided into four categories, which reflect the evolution of the parameter: (1) a constant value of LUE<sub>max</sub> for global vegetation; (2) specific LUE<sub>max</sub> values for each vegetation type or biome; (3) specific LUE<sub>max</sub> values for C4 and C3 plants; and (4) specific LUE<sub>max</sub> values for sunlit and shaded leaves (He et al. 2013; Myreni et al. 1995; Potter et al. 1993; Prince and Goward 1995; Zhang et al. 2017; Zhao et al. 2005).

In the early 1990s, a constant LUE<sub>max</sub> of 0.39 gC/MJ was used across the globe (Myreni et al. 1995; Potter et al. 1993). While more studies considered that the LUE<sub>max</sub> varies with ecological, physical, and environmental factors, including PFTs, stomatal conductance, illumination angle, and stress levels (Madani et al. 2014; Zhao et al. 2005). For example, the MODIS Biome Properties Look-Up Table (BPLUT) prescribes a LUE<sub>max</sub> value for 11 biomes, and this BPLUT has been widely adopted by various models (Zhao et al. 2005). The VPM and GLO-PEM models use different LUE<sub>max</sub> values for C3 and C4 plants (Prince and Goward 1995; Zhang et al. 2017). For instance, the LUE<sub>max</sub> values of C3 and C4 plants are set as 0.42 and 0.63 g/mol APAR respectively in the latest VPM GPP products (Zhang et al. 2017). Some studies have considered the difference of LUE<sub>max</sub> for sunlit and shaded leaves, as well as for cloudy and clear days. For instance, He et al. (2013) demonstrated that the LUE<sub>max</sub> for shaded leaves is 2.5 to 3.8 times larger than that for sunlit leaves at 6 eddy flux tower sites across China.

LUE<sub>max</sub> can be defined in three different ways, by using incident

radiation ( $LUE_{inc}$  or  $LUE_{max}^{eco}$ ), incident radiation absorbed by vegetation ( $LUE_{total}$  or  $LUE_{max}^{canopy}$ ), and incident radiation absorbed by chlorophyll ( $LUE_{green}$  or  $LUE_{max}^{chl}$ ) (Gitelson and Gamon 2015; Zhang et al. 2018a). One study compared these three forms of  $LUE_{max}$  at 127 eddy flux sites and found that daily  $LUE_{max}^{chl}$  tends to converge across biomes for all C3 plants (Zhang et al. 2018a). This conclusion justifies that a constant  $LUE_{max}^{chl}$  can be applied for the parameterization of LUE models as it avoids the data/parameters input of vegetation types and reduces the uncertainty, and thus it ultimately improves the accuracy of GPP estimation. Thus, the currently used  $LUE_{max}$  values do not have a common basis, which leads to limitations for comparative analyses of reported  $LUE_{max}$ , and the reported  $LUE_{max}$  values can vary a lot over a wide range (Gitelson and Gamon 2015; Zhu et al. 2016; Zhu et al. 2018).

### 3.4. Environmental stress factors for light use efficiency: representability and integrity

The evolution of the environmental stress factors includes the improvements in (1) the proxy selection and representation of environmental stress factors, and (2) the integration forms of environmental stress factors

#### 3.4.1. Proxy selection and representation of environmental stress factors

**3.4.1.1. Temperature scalar.** Low or high air temperature can decrease enzyme activity and slow the processes of photosynthesis. The proxies of temperature stress used in the LUE models mainly include three variables: daily mean air temperature ( $f(T_a)$ ), daily minimum air temperature ( $f(T_{min})$ ), and land surface temperature ( $f(LST)$ ). The  $f(T_a)$  is the most widely used proxy in the existing models, such as the GLO-PEM, 3-PG, C-Fix, VPM, EC-LUE, TL-LUE, TL-LUEn, TEC, MVPM, CI-LUE, MuSyQ, CCW, TCF, DTEC, and Wang's model (Table 1). The  $f(T_{min})$  represents the minimum temperature at which photosynthesis occurs and is used in MOD17, CFLUX, and CI-LUE models (Table 1). The  $f(LST)$  can be directly obtained from remote sensing data and is usually adopted by models that simulate large-scale spatially continuous GPP, such as the TG model.

The temperature stress functions in the LUE models usually fall into one of three categories: (1) minimum, maximum, and optimum temperature ( $f(T_{min}, T_{opt}, T_{max})$ ) are considered, which is done in the Terrestrial Ecosystem Model (TEM) and VPM model; (2) only daily minimum temperature ( $f(T_{min})$ ) is considered, such as in MOD17; and (3) only optimum temperature ( $f(T_{opt})$ ) is considered, such as in MuSyQ. One study has compared the performances of these three methods of approximating temperature stress in LUE models in different vegetation types and demonstrated that  $f(T_{min}, T_{opt}, T_{max})$  and  $f(T_{opt})$  show no significant difference in model performance and that  $f(T_{min})$  exhibits better performance than  $f(T_{min}, T_{opt}, T_{max})$  and  $f(T_{opt})$ , particularly for croplands (Zheng et al. 2018).

**3.4.1.2. Water stress scalar.** The proxies of water stress can be classified into three types: (1) atmospheric water stress, often measured with vapor pressure deficit (VPD), relative humidity (RH), specific humidity deficit (SHD), and precipitation (Pre); (2) soil water stress, often measured with soil water saturation (SWS), soil water content (SWC), and soil moisture (SM); and (3) plant water stress, often measured with Land Surface Water Index (LSWI), plant evaporative fraction (EF), and plant moisture (PM).

Atmospheric water affects evapotranspiration and photosynthesis by controlling stomatal conductance (Ocheltree et al. 2014). It is the most used water stress factor seen in models such as MOD17, 3-PG, CFLUX, EC-LUE, TL-LUE, TL-LUEn, TCF, MVPM, CCW, CI-LUE, Wang's model. Apart from VPD,  $f(SHD)$  is also used as a proxy of atmospheric water stress, such as the GLO-PEM model.

Soil water couples the water vapor demand of the atmosphere and

the water supply from soil to leaves via roots (Leuning et al. 2005). Soil provides a buffer between water gained from precipitation and water loss by evapotranspiration. A recent study determined that declines in soil moisture alone reduced annual GPP by up to 40% in arid/semi-arid regions (Stocker et al. 2018). Thus, soil moisture availability is an important factor affecting GPP. Both the SM factor ( $f(SM)$ ) and SWC factor ( $f(SWC)$ ) have been used in LUE models such as GLO-PEM, 3-PG, CFLUX, and Wang's model (Table 1). Studies have shown that SWC performs better in explaining LUE variations in grasslands than forests and shrubs (Zhang et al. 2015b). This difference can be explained by the fact that woody plants have higher water accessibility via deep roots (Canadell et al. 1996; Schenk and Jackson 2002) and store more water in their stems (Schenk and Jackson 2002; Sims et al. 2014), which serve to decrease the sensitivity of LUE to variances in shallow soil moisture.

Plant water stress affects stomatal conductance and regulates the exchange of water and CO<sub>2</sub> between the leaves and the atmosphere. Leaf water content is an indicator of plant water stress. The LSWI obtained directly from remote sensing data ( $f(LSWI)$ ) has been widely used as a proxy of plant water stress, such as in the VPM, MVPM, and PCM models (Table 1). EF ( $f(EF)$ ), which describes the plant water status through the regulation of sensible and latent heat fluxes, has been used to represent plant water stress in EC-LUE and CI-EF models (de Almeida et al. 2018; Yuan et al. 2010; Yuan et al. 2007; Yuan et al. 2019). PM ( $f(PM)$ ) uses the relationship between FPAR and the maximum FPAR to reflect plant water status, and Wang et al. (2018) use  $f(PM)$  in their model to estimate GPP. In addition, the ratio of evapotranspiration (E) and potential evaporation (E<sub>p</sub>) ( $f(E/E_p)$ ) has been employed to represent the water stress in TEC, MuSyQ, and DTEC models (Table 1).

Zhang et al. (2015b) investigated the effects of different water indicators (including SWC, SWS, LSWI, EF, VPD, and precipitation) on LUE for a wide range of ecosystems on daily, 8-day, and monthly scales based on FLUXNET and MODIS data. They found that LUE is more responsive to plant water indicators (EF and LSWI) than to soil water indicators (SWC and SWS) and atmospheric water indicators (VPD and precipitation) (Zhang et al. 2015b) (Fig. 3). These findings suggest that plant water stress indicators are preferred in LUE models (Garbulsky et al. 2010; Yuan et al. 2007; Zhang et al. 2015b; Zheng et al. 2018).

In addition to using different indicators to characterize water stress, the LUE models also use different equations to calculate water stress scalars (Table 1). Note that some models do not use any water stress factors, such as the C-Fix and DIFFUSE models (Table 1), as these models are usually used in humid temperate (e.g., Europe) or tropical (e.g., Australia) regions.

**3.4.1.3. CO<sub>2</sub> scalar.** Atmospheric CO<sub>2</sub> concentration is an important factor that affects the photosynthetic efficiency due to the CO<sub>2</sub> fertilization effect. But only a few LUE models consider the CO<sub>2</sub> fertilization effect (e.g., the EC-LUE and C-Fix models). The C-Fix model considered the effects of CO<sub>2</sub> fertilization (Veroustraete et al. 2002) by the ratio of CO<sub>2</sub> assimilation rate to the CO<sub>2</sub> concentration (281 ppm) in the reference year of 1833 (Collatz et al. 1991). Yuan et al. (2019) improved the CO<sub>2</sub> concentration scalar in the revised EC-LUE model by a function of the CO<sub>2</sub> compensation point, CO<sub>2</sub> concentration in the intercellular air spaces of the leaf, the atmospheric CO<sub>2</sub> concentration, and the ratio of leaf internal to ambient CO<sub>2</sub> (Collatz et al. 1991; Farquhar et al. 1980). A most recent study showed the CO<sub>2</sub> fertilization effect in the EC-LUE model can improve estimates of global GPP for reproducing its long-term variation (Zheng et al. 2020).

**3.4.1.4. Other scalars.** Biological factors (e.g., forest stand age,  $f(SA)$ ) are integrated into some LUE models, such as the Physiological Principles in Predicting Growth (3-PG) (Landsberg and Waring 1997; Marques Caldeira et al. 2020) and CFLUX models. In forest ecosystems,  $f(SA)$  can be considered a factor for GPP as the above-ground biomass varies with forest age within a certain range. The effects of stand age can be

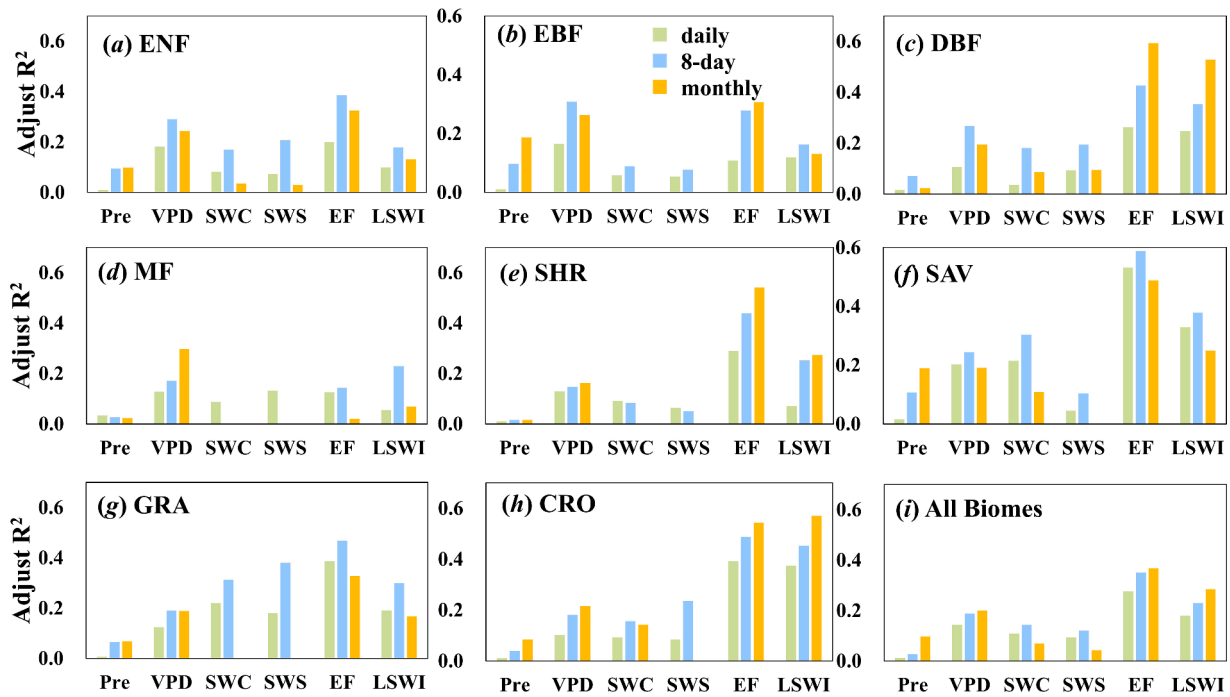


**Fig. 3.** Adjusted  $R^2$  between LUE and water indicators for (a-h) different biomes and (i) all biomes on daily, 8-day, and monthly scales derived from 253 eddy covariance (EC) towers. Atmospheric water indicators: precipitation (Pre), and daytime vapor pressure deficit (VPD), were derived from EC flux sites; Plant water indicators: land surface water index (LSWI) and evaporative fraction (EF), were derived from MODIS reflectance data (MOD09A1) and EC flux sites, respectively; Soil water indicators: volumetric soil water content (SWC) and soil water saturation (SWS), were derived from EC flux sites and a global high-resolution soil data set (Shangguan et al. 2014), respectively. IGBP Biome abbreviations: ENF (evergreen needleleaf forest), EBF (evergreen broadleaf forest), DBF (deciduous broadleaf forest), MF (mixed forest), SHR (close shrub and open shrub), SAV (savannas and woody savannas), GRA (grassland), and CRO (cropland). (Adapted from Zhang et al. (2015b)).

considered as an empirical expression of relative stand age (RSA) which is defined as the ratio of actual age to the maximum age in the 3-PG model (Landsberg and Waring 1997). That can also be considered by using an alternative indicator of the ratio of GPP to  $GPP_{max}$  in the CFLUX model (Turner et al. 2006; Turner et al. 2009).

Some models also consider the effect of freezing conditions ( $f(FT)$ ) on landscape water mobility and photosynthesis, such as the TCF model (He et al. 2016; Yi et al. 2013). The  $f(FT)$  is usually set to 0 (fully constrained) under frozen landscape conditions, 0.5 (partially constrained) for transitional FT days, and 1 (no constraint) under non-frozen conditions (He et al. 2016; Yi et al. 2013).

#### 3.4.2. Integration of environmental stress factors

Generally, more environmental stress factors were considered in the evolution of the LUE GPP models. Most LUE GPP models integrate 2 or 3 environmental stress factors, such as the GLO-PEM, MOD17, TEC, and MuSyQ models. Temperature ( $f(T)$ ) and water ( $f(W)$ ) stress factors are used by nearly all the LUE GPP models. Some models account for up to 4 or 5 environmental stress factors. For instance, the TCF model includes 4 environmental stress factors, including air temperature  $f(T_a)$ , vapor pressure deficit  $f(VPD)$ , soil moisture  $f(SM)$ , and  $f(FT)$  (He et al. 2016). Wang et al. (2018) considers 5 environmental stress factors, including  $f(T_a)$ , plant moistures such as  $f(PM)$ ,  $f(VPD)$ , soil water content  $f(SWC)$ , and cloudiness index  $f(CI)$ .

In terms of integrating environmental stress factors, most LUE models use the multiplication method to integrate environmental stress factors, such as GLO-PEM, MOD17, C-Fix, VPM, TL-LUE, TL-LUEN, PCM, TEC, CI-LUE, MuSyQ, TCF, DTEC, CI-EF, and Wang's model (Table 1). However, some studies show that the law of the minimum (LOM) introduced into the model is also useful, e.g., 3-PG, CFLUX, EC-LUE, MVPM, and CCW models. These models have different strategies when applying the LOM method. For example, the EC-LUE and MVPM models only consider the lesser of the temperature and water effects as the

constraint factor for photosynthesis. The CCW model considers other stress factors, such as clouds (Zhang et al. 2016b). In addition, some models include different indicators for the same environmental factor. For example, the smaller of  $f(SM)$  and  $f(VPD)$  is identified as the water scalar in the 3-PG and CFLUX models.

#### 4. Model Uncertainties

Despite the substantial advances in recent decades, the LUE-based GPP models still have some uncertainties (Anav et al. 2015; Schaefer et al. 2012), due to differences in model structures and parameterization, uncertainties in input and validation data, and scale mismatch.

##### 4.1. Effects of model structure and parametrization on GPP simulation accuracy

Although LUE-based GPP models are all based on LUE logic (Eq.1), they have different structures, which have been attributed as the most important factor affecting model performance (Yuan et al. 2014). Zhang et al. (2015a) evaluated the performance of 4 LUE models at 51 eddy covariance flux towers and found that structure optimization through adding one more water stress scalar (i.e., VPD) and using the LOM method between VPD and LSWI in the model can improve the VPM GPP estimates.

Many studies have examined the effects of different LUE model components on GPP estimation. Different representations for FPAR and environmental stresses (Zheng et al. 2018) could greatly affect GPP estimation. For example, the FPAR in the LUE models is usually represented as a linear relationship with vegetation indices (e.g., NDVI and EVI). This assumption could introduce some uncertainties in GPP estimation (Running et al. 2000). The current environmental stress factors in the LUE models, on one hand, may not capture some other features naturally, such as root distribution, drought adaptation strategy,

nutrient constraint, land management, and vegetation disturbance, which may result in some bias in GPP estimation (Klein et al. 2014; Reyer et al. 2013). On the other hand, more environmental stress factors could have interactions among themselves, which in turn could introduce more uncertainties in data quality and parameterization.

The uncertainties of the parameterization scheme in the LUE models significantly influence model performance (Wagle et al. 2016). Xiao et al. (2014) quantified the uncertainty of model parameters and assessed its effects on the estimation of regional carbon fluxes. They found that the parameterization of  $LUE_{max}$  could substantially affect GPP estimation. The  $LUE_{max}$  in an ecosystem on an annual scale is usually on the order of 2% under ideal growing conditions (Baldocchi and Penuelas 2019). The highest  $LUE_{max}$  appears in the wet tropics, which are characterized by favorable growing temperatures, ample water availability, long growing seasons, and a high ratio of diffuse light. The  $LUE_{max}$  values are controversial and range from 0.62 to 14.89 g C m<sup>-2</sup> MJ<sup>-1</sup> APAR in previous studies (Yuan et al. 2014). Also, how much the actual LUE deviates from the  $LUE_{max}$  remains highly uncertain and is affected by the parameters in the LUE models, such as the maximum, minimum, and optimal temperatures, and proxies of water stress.

#### 4.2. To what degree do input data and validation data matter?

The spatial resolutions and accuracies of input datasets could introduce considerable uncertainties in GPP simulations (Zhao et al. 2006). The input datasets for LUE models mainly include gridded remote sensing datasets and meteorological datasets (Cai et al. 2014a; Zhao et al. 2006). The remote sensing datasets mainly include the land cover, vegetation index data (e.g., NDVI, EVI, FPAR, PRI), and SIF. Land cover maps are usually derived from satellite data and substantial uncertainties exist due to their data sources, classification schemes, and classifiers (Giri et al. 2005). For a given site or grid cell, the land cover type directly determines the value of  $LUE_{max}$ . Remotely sensed indices (e.g., LAI, NDVI, and EVI) are often contaminated by atmospheric interference, which may contribute a misleading signal when vegetation becomes stressed, e.g., green canopies that are not photosynthesizing (Frankenberg et al. 2011). Also, the uncertainties caused by sensor degradation, signal-to-noise ratio (SNR), and spatial/temporal resolution for remote sensing data also deserve attention. For example, a previous study showed that the MODIS FPAR tended to be underestimated and displayed larger seasonal variations in old forests (Serbin et al. 2013).

The meteorological datasets mainly include temperature, precipitation, soil moisture, and PAR data. The uncertainties of meteorological products are also likely to be propagated to GPP estimation (Heinsch et al. 2006). For example, the meteorological datasets used to derive PAR involve substantial uncertainties. The commonly used PAR datasets for GPP estimation include the National Center for Environmental Prediction-Department of Energy (NCEP-DOE) Reanalysis II, World Meteorological Organization (WMO), Modern-Era Retrospective Analysis for Research and Applications (MERRA), ERA-Interim, Climatic Research Unit (CRU-NCEP), Global Land Surface Satellite Product (GLASS), and the European Centre for Medium-Range Weather Forecasts (ECMWF) (Yuan et al. 2019; Zhu et al. 2016). The NCEP-DOE Reanalysis II meteorology data are found ineffective for estimating PAR when compared to site data (Zhu et al. 2016). Jung et al. (2011) compared four remote sensing-based global solar radiation products and reported a consistent overestimation in the magnitudes, but with different trends and interannual variabilities. Cai et al. (2014b) examined the impacts of the different radiation products on GPP estimates in China and found that GPP simulation driven by the GLASS radiation product had the highest model performance when compared with the estimated GPP from the EC tower sites ( $GPP_{EC}$ ).

Downward shortwave radiation at the surface is often converted to PAR using a constant ratio, such as 0.5 or 0.45. An invariant ratio,

however, inevitably involves uncertainties since the ratio varies with altitude, view zenith angle, and water vapor content (Ryu et al. 2018). Ryu et al. (2018) proved that the ratio varies from 0.41 to 0.53 on an annual mean scale across the global land surface. Solar radiation is not used as an explanatory variable in the machine learning based global GPP products due to its high uncertainties.

Uncertainty also exists in the validation. The EC flux tower measurements have been used as the main source for the validation of GPP estimates. However, the flux tower based GPP estimates also have uncertainties. The reference GPP based on flux tower measurements is derived from EC-measured net ecosystem exchange data through partitioning and gap-filling, which can introduce certain biases (Reichstein et al. 2005). Previous studies showed that the tower-based reference GPP is subject to have 10%–30% errors due to these methods (Reichstein et al. 2005; Schaefer et al. 2012). These biases can also affect model calibrations and performances. Also, the uncertainties in tower-based GPP estimations may propagate to other related variables, such as the actual LUE derived from flux tower GPP (Zhang et al. 2015b), and trigger some inherited uncertainties.

#### 4.3. Effects of Scale Mismatch

The spatial-temporal scale mismatch of input datasets and parameters can be another source of uncertainties. First, a scale mismatch exists between the input datasets. The coarse-resolution meteorological data (e.g., temperature and solar radiation, 0.5° to 2°) and moderate-resolution remote sensing data (e.g., NDVI, EVI, FPAR, and LAI, 500 m to 1 km) have a scale mismatch. As a result, the substantial scale mismatch between the atmosphere and land surface forcing leads to errors in GPP estimation (Running et al. 2004; Yuan et al. 2010). Although strict interpolation and resampling are used to make the resolutions of these climate datasets comparable to that of the remote sensing products, the uncertainties could not be eliminated (Zhu et al. 2016).

Second, the scale mismatch exists between the flux tower “footprint” and the remote sensing data. The tower-based reference GPP estimations represent a flux integrated over the tower “footprint”, the size and shape of which depend on wind speed, wind direction, surface roughness, and atmospheric stability (Turner et al. 2003). Typical flux tower footprints have longitudinal length scales of 100–2000 m (Baldocchi et al. 2001), while the spatial resolutions of remote sensing products are usually at 500–8000 m. Spatially averaged MODIS reflectance values from 3 × 3 grid cell windows over each tower location have been used to reduce these effects, but this practice may introduce additional uncertainties through regional smoothing of MODIS retrievals and model simulations relative to local tower observations, especially over spatially complex vegetation and terrain.

### 5. Implications for the future

#### 5.1. Complexity or simplicity?

Generally, the LUE models have evolved to be more sophisticated with higher complexity. The components of LUE models, i.e., PAR, FPAR, environmental stress factors, and  $LUE_{max}$  have evolved as described in Section 3. The evolution of the LUE models has generally improved the accuracy of GPP estimation. These evolving characteristics have further clarified and improved the theoretical mechanism of the LUE models, which can depict the details of the LUE models when simulating terrestrial GPP. For example, many environmental stress factors in the LUE models clarified the various environmental factors that limit GPP, like temperature, water, freezing conditions, stand age, and CO<sub>2</sub>. However, attention should also be paid to the uncertainties caused by introducing more parameters and more components, which could also increase the uncertainty of LUE models.

Recently, the emergence of new indicators, such as the

photochemical reflectance index (PRI), sun-induced chlorophyll fluorescence (SIF), and near-infrared reflectance of terrestrial vegetation (NIRv), may facilitate GPP simulation using simpler statistical methods. For example, the PRI is sensitive to changes in xanthophyll pigments (Drolet et al. 2005; Gamon et al. 1992) and thus can be directly used as an indicator or proxy for actual LUE in GPP estimation. SIF is energy emitted by plant chlorophyll in the 600 – 800 nm wavelength range after light absorption, which is highly correlated with photosynthesis at coarse spatiotemporal scales when non-photochemical quenching dominates at high light levels (Baker 2008; Magney et al. 2020a).

SIF is considered to contain information about both APAR and LUE (Yang et al. 2015). Many studies have shown that SIF alone may improve the predictive power of estimating GPP compared to other GPP models that require several types of input data, especially under drought conditions (Guanter et al. 2014). NIRv is the product of NIR reflectance and NDVI and represents the proportion of reflectance attributable to vegetation (Badgley et al. 2017a). NIRv has been used to estimate global GPP without additional information on environmental conditions (such as precipitation, temperature, VPD, or PAR) (Badgley et al. 2019; Badgley et al. 2017a). The simplification of actual LUE directly by PRI and the simplification of GPP estimation directly by SIF and NIRv have been shown to be applicable at different FPAR levels (i.e., canopy vs. leaf) (Gamon and Berry 2012; Hilker et al. 2009; Stagakis et al. 2014; Zhang et al. 2016a), radiation levels (i.e., sunny days vs. cloudy days) (Yang et al. 2015), timescales (i.e., daily vs. seasonal) (Li et al. 2018a; Li et al. 2018b; Zhang et al. 2016c; Zhang et al. 2018b), and PFTs (Badgley et al. 2019; Baldocchi et al. 2020; Damm et al. 2015; Drolet et al. 2005; Drolet et al. 2008; Duveiller and Cescatti 2016; Filella et al. 2009; Garbulsky et al. 2011; Garbulsky et al. 2008; Goerner et al. 2011; Penuelas et al. 2011; Wu et al. 2020; Zhang et al. 2016a). However, SIF and GPP can become decoupled when vegetation becomes stressed (Helm et al. 2020; Marrs et al. 2020) and NIRv and SIF have been shown to have little to no correlation in the tropics (Doughty et al. 2021).

These evolving methods of estimating GPP show that: (1) the complexity of LUE GPP models tends to increase with improvements in our understanding of PAR, FPAR,  $LUE_{max}$ , and environmental stress factors, and (2) there is a tendency towards simplicity in the calculation of GPP with the advent of new vegetation indicators (e.g., PRI, SIF, and NIRv). In fact, a set of SIF-based GPP estimates have been released in recent years (Li and Xiao 2019; Wang et al. 2021). The selection of GPP models depends on our specific targets and conditions. We may need the more sophisticated LUE models if we aim to identify key limitation factors and estimate GPP at relatively high spatial and temporal resolutions. While the SIF-based models can offer a good option for quick approximations of GPP at coarse spatial and temporal scales, they fail to disentangle the factors driving the photosynthesis (Magney et al. 2020b; Zhang et al. 2016c).

## 5.2. Implications for future LUE-based GPP models

Given the trends in the evolution of LUE models and the uncertainties we identified in this review, we raise some issues that deserve attention in the future LUE GPP model improvement.

First, there is a lack of a comprehensive LUE model that integrates all the current evolutionary features. For example, the TL-LUE model considered the shaded and sunlit leaves, but only considered the temperature and water stress factors (He et al. 2013). The DIFFUSE model only considered radiation conditions, without distinguishing different FPAR levels or considering any environmental stress factors (Donohue et al. 2014). The more environmental stress factors in an LUE model may more comprehensively quantify environmental stress. However, there may be synergistic changes among different environmental stress factors, which may decrease the accuracy of the models. More studies are needed to identify optimized factors for the LUE models by considering the trade-offs of fewer factors-caused errors and more factors-caused uncertainties in GPP estimation. The machine learning models are

usually based on artificial neural networks, random forest algorithms, and/or multivariate adaptive regression splines for upscaling the site-level measurements to the regional or global scales, such as EC-Moderate Resolution Imaging Spectroradiometer (EC-MOD), model tree ensembles (MTE) or regression tree (RT) approaches (Jung et al. 2009; Jung et al. 2011; Tramontana et al. 2016; Xiao et al. 2010; Yang et al. 2007). The machine learning methods use the intrinsic observational nature between the measurements and the explanatory variables to build the functional relationships (Tramontana et al. 2016). The combination of LUE models and machine learning methods may also be an important direction for accurate simulation of terrestrial GPP in the future.

Second, the water stress factors have complex effects on GPP estimates, such that a single indicator or function may not sufficiently capture the diverse responses of plants to water stresses, especially under drought conditions. No indicator is found to explain the LUE variation stressed by water as much as expected. The representative indicators from the atmosphere (VPD), soil (SWC), and plant (EF) water indicators only explain 20%, 6%, and 36% of LUE variations on the monthly scale (Zhang et al. 2015b), further reflecting the complexity of water stress on canopy photosynthesis (Churkina et al. 1999). Those LUE GPP models that are only based on VPD can explain the effects of atmospheric water demand regulating leaf stomatal closure and canopy gas exchange, but cannot evaluate impacts from soil water supply variations (Leuning et al. 2005). Although plant water indicators perform better than atmosphere and soil water indicators in explaining LUE variation, the unavailability over space (e.g., EF) and the frequent cloud contamination (e.g., LSWI) limit their applications in LUE models (Xiao et al. 2004a; Xiao et al. 2004b; Yuan et al. 2007). In the future, LUE models can integrate multiple water stress factors to capture the environmental controls more realistically on ecosystem functions. For example, the Soil Moisture Active Passive (SMAP) data and the following SMAP-Sentinel-1 combined soil moisture data provide unprecedented information on soil moisture (Reichle et al. 2019), which could significantly enhance our understanding of global soil water stress on LUE and further improve GPP estimation.

Third, the emerging PRI, SIF, and NIR<sub>v</sub> indicators may play an important role in improving the accuracy of LUE models in regional and global GPP simulations. A recent study has already shown that the combination of PRI and SIF can be used to improve the accuracy of GPP estimation at 61 sites distributed globally (Wang et al. 2020). Integrating the PRI and SIF indicators into the calibration of LUE models, together with the evolution characteristics of LUE models, may be a direction for improvement of the LUE model in the future (Perez-Priego et al. 2015).

## 6. Conclusions

In this study, we reviewed 21 LUE-based GPP models to understand their evolution and uncertainties. We found that, on one side, the LUE models became more sophisticated in terms of each component of PAR, FPAR,  $LUE_{max}$ , and environmental stress factors. Specifically, PAR evolved from total PAR to direct PAR and diffuse PAR. FPAR has evolved from one-leaf to two-leaf and from canopy to chlorophyll level FPAR. The  $LUE_{max}$  has evolved from a constant value to specific values for each vegetation type, C4 and C3 plants, and sunlit and shaded leaves. The number and complexity of environmental stress factors has also increased. On the other side, the emerging PRI, SIF, and NIRv data have simplified methods to estimate GPP, through the simplification of actual LUE directly by PRI or the simple scaling of SIF and NIRv to GPP. The LUE models are more helpful in understanding the driving mechanisms of the variances in GPP, while emerging new indicators, such as SIF, are more conducive to the rapid monitoring of terrestrial GPP. The selection of more complex LUE models or simpler proxies of GPP will depend on specific targets and conditions. The integration use of the LUE models with the new indicators may serve as a new direction for future model

developments. For example, the newly acquired and forthcoming SIF data, such as from the TROPOspheric Monitoring Instrument (TROPOMI) and the Geostationary Carbon Observatory (GeoCarb), are expected to greatly help the future development of LUE-based GPP models.

#### Declaration of Competing Interest

The authors declare that they have no known competing financial interests or personal relationships that could have appeared to influence the work reported in this paper.

#### Appendix: Acronym table

3-PG	the Physiological Principles in Predicting Growth activation energy in C-Fix model.
AE	
APAR <sub>sh</sub>	the PAR absorbed by the shaded leaves.
APAR <sub>su</sub>	the PAR absorbed by the sunlit leaves.
C	quantifies the contribution of multiple scattering of the total PAR to the diffuse irradiance per unit leaf area within the canopy.
C <sub>1</sub>	constant in C-Fix model.
C <sub>a</sub>	the atmospheric CO <sub>2</sub> concentration.
CCW	Coupled Carbon and Water model
C-Fix	Carbon Fix model
CFLUX	carbon flux model
Chl	Chlorophyll content.
C <sub>i</sub>	the CO <sub>2</sub> concentration in the intercellular air spaces of the leaf (ppm).
CI	cloudiness index.
CI <sub>d</sub>	cloudiness index for the specific day.
CI-EF	cloudiness index-Evaporative Fraction model
CI-LUE	cloudiness index-light use efficiency model
CI <sub>max</sub>	the maximum CI.
CI <sub>min</sub>	the minimum CI.
D <sub>0</sub>	empirical coefficient for VPD in Wang's model, and D0=15 hPa.
DE	deactivation energy in C-Fix model.
D <sub>f</sub>	diffuse fraction, the ratio of the diffuse (R <sub>d</sub> ) to shortwave irradiance (R <sub>s</sub> ).
DTEC	Diffuse Fraction-Based Two-Leaf Light Use Efficiency Model
E	the actual evapotranspiration.
EC-LUE	Eddy-Covariance light use efficiency model.
ECMWF ERA	European Centre for Medium-Range Weather Forecasts (ECMWF) ERA-Interim reanalysis data.
EF	plant evaporative fraction
EN	entropy of the denaturation equilibrium of CO <sub>2</sub> in C-Fix model.
EP	the Priestley and Taylor (1972) potential evaporation.
EVI	Enhanced Vegetation Index
f(CI)	cloudiness index factor
f(CO <sub>2</sub> )	atmospheric CO <sub>2</sub> concentration factor.
f(EF)	evaporative fraction factor.
f(PM)	plant moisture constraint, defined as the ratio of FPAR to FPAR <sub>max</sub>
f(SA)	Stand Age factor.
f(W)	Water scalar
f(VPD)	the VPD constraint reflecting the stomatal response to the atmospheric water saturation deficit
f(SWC)	the soil moisture constraint on the photosynthesis
f <sub>a</sub>	the green canopy fraction indicating the proportion of active canopy
f <sub>M</sub>	the plant moisture constraint
f(T <sub>a</sub> )	the air temperature constraint reflecting the temperature limitation of photosynthesis
f(TM <sub>IN</sub> )	the minimum temperature factor
F <sub>CO<sub>2</sub></sub>	the CO <sub>2</sub> assimilation rate.
F <sub>CO<sub>2</sub></sub> <sup>ref</sup>	the CO <sub>2</sub> concentration occurring in the reference year 1833 being equal to 281 ppmv in C-Fix model.
FD	frost days per month.
FPAR	Fraction of absorbed Photosynthetically Active Radiation
GC	gas constant in C-Fix model.
GLO-PEM	Global Production Efficiency Model.
GPP <sub>c</sub>	conductance-limited GPP
GPP <sub>r</sub>	radiation-limited GPP, which estimated using a LUE model
GR	Greenness and Radiation model
H	sensible heat
h, c	power and coefficient in f(SM) in 3-PG.
k	empirical coefficient, describing the relationship between stomal and canopy conductance and VPD in 3-PG.
LAI <sub>sh</sub>	the LAI of shaded leaves.
LAI <sub>su</sub>	the LAI of sunlit leaves.
LE	latent heat
LST <sub>an</sub>	the mean annual night Land Surface Temperature.
LSWI	the Land Surface Water Index
LSWI <sub>max</sub>	the maximum LSWI during the growing season for each pixel.
LUE	Light Use Efficiency
m	a scalar with the unit of mol C m <sup>-2</sup> day <sup>-1</sup> in GR, TG and VI model.

#### Acknowledgment

This study is funded by the Strategic Priority Research Program (XDA19040301) of the Chinese Academy of Sciences (CAS), the National Natural Science Foundation of China (NSFC) (42001378), the Key Research Program of Frontier Sciences (QYZDB-SSW-DQC005) of the Chinese Academy of Sciences (CAS), and U.S. National Science Foundation (1946093).

(continued on next page)

(continued)

MODIS	Moderate Resolution Imaging Spectroradiometer
MuSyQ-GPP	Multi-source data Synergized Quantitative-GPP algorithm
MVPM	modified Vegetation Photosynthesis Model
<i>n</i>	empirical power term in 3-PG.
NDVI	Normalized Difference Vegetation Index
PAR	Photosynthetically Active Radiation
PAR <sub>c</sub>	the PAR intercepted by the canopy.
PAR <sub>dif</sub>	the diffuse component of incoming PAR.
PAR <sub>dif,u</sub>	the diffuse PAR under the canopy.
PAR <sub>dir</sub>	the direct component of incoming PAR.
PAR <sub>po</sub>	the potential incident PAR
PCM	Photosynthetic Capacity Model
PC <sub>max</sub>	the maximum photosynthetic capacity.
PRI	Photochemical Reflectance Index
<i>R</i>	the sky clearness index
R <sub>n</sub>	net radiation.
R <sub>s</sub>	the diffuse radiation scalar
RSA	relative stand age, defined as actual age/estimated maximum age.
S <sub>0</sub>	the solar constant (1367 W m <sup>-2</sup> ).
SH	the specific humidity of the air.
SHD	specific humidity deficit (g kg <sup>-1</sup> ).
SI	sky clearness index.
SM	soil moisture.
SSH	the saturated specific humidity at the air temperature.
SVI	Scaled vegetation index.
SWC	soil water content.
SWC <sub>max</sub>	the maximum of soil water content.
SWS	soil water saturation
Ta	air temperature
TCF	Terrestrial Carbon Flux model
TD	total number of days per month.
TEC	terrestrial ecosystem carbon flux model
TEM	Terrestrial Ecosystem Model
TG	Temperature and Greenness model
TL-LUE	Two-Leaf Light Use Efficiency Model
TL-LUEn	Nonlinear Two-Leaf Light Use Efficiency Model
T <sub>MIN</sub>	the minimum temperature.
T <sub>opt</sub>	the optimum air temperature (°C) for photosynthetic activity.
TPM	Two-Parameter Model
T <sub>s</sub>	the temperature stress
VI	Vegetation Index Model
VPD	vapor pressure deficit
VPM	Vegetation Photosynthesis Model
VPRM	Vegetation Photosynthesis and Respiration Model
W <sub>s</sub>	the water stress
$\alpha$	the albedo related to vegetation types.
$\beta$	Bowen ration, defined as the ratio of energy available for sensible heating (H, W m <sup>-2</sup> ) to energy available for latent heating (LE, W m <sup>-2</sup> ).
$\varepsilon_{base}$	the base light use efficiency.
$\varepsilon_{cs}$	the light use efficiency for clear sky days.
$\varepsilon_m$	the quantum yield when incident PAR approaches zero.
$\varepsilon_{msh}$	the maximum LUE of shaded leaves.
$\varepsilon_{msu}$	the maximum LUE of sunlit leaves.
$\theta$	the CO <sub>2</sub> compensation point in the absence of dark respiration (ppm)
$\lambda$	the mean leaf-sun angle and set as 60°
$\mu$	indicates an overall sensitivity of GPP to CI in Wang's model.
$\tau$	the maximum canopy photosynthetic flux density at light saturation.
$\varphi$	the solar zenith angle.
$\chi$	the ratio of leaf internal to ambient CO <sub>2</sub> .
$\Omega$	the clumping index.

## References

- Anav, A., Friedlingstein, P., Beer, C., Ciais, P., Harper, A., Jones, C., Murray-Tortarolo, G., Papale, D., Parazoo, N.C., Peylin, P., Piao, S., Sitch, S., Viovy, N., Wilshire, A., Zhao, M., 2015. Spatiotemporal patterns of terrestrial gross primary production: a review. *Rev. Geophys.* 53, 785–818.
- Badgley, G., Anderegg, L.D.L., Berry, J.A., Field, C.B., 2019. Terrestrial gross primary production: using NIRV to scale from site to globe. *Global Change Biol.* 25, 3731–3740.
- Badgley, G., Field, C.B., Berry, J.A., 2017a. Canopy near-infrared reflectance and terrestrial photosynthesis. *Sci. Adv.* 3.
- Badgley, G., Field, C.B., Berry, J.A., 2017b. Canopy near-infrared reflectance and terrestrial photosynthesis. *Sci. Adv.* 3, e1602244.
- Baker, N.R., 2008. Chlorophyll fluorescence: a probe of photosynthesis *in vivo*. *Annu. Rev. Plant Biol.* 59, 89–113.
- Baldocchi, D., 2014. Measuring fluxes of trace gases and energy between ecosystems and the atmosphere - the state and future of the eddy covariance method. *Global Change Biol.* 20, 3600–3609.
- U, K.T.P. Baldocchi, D., Falge, E., Gu, L.H., Olson, R., Hollinger, D., Running, S., Anthroni, P., Bernhofer, C., Davis, K., Evans, R., Fuentes, J., Goldstein, A., Katul, G., Law, B., Lee, X.H., Malhi, Y., Meyers, T., Munger, W., Oechel, W., Pilegaard, K., Schmid, H.P., Valentini, R., Verma, S., Vesala, T., Wilson, K., Wofsy, S., 2001. FLUXNET: a new tool to study the temporal and spatial variability of ecosystem-scale carbon dioxide, water vapor, and energy flux densities. In: *Bull. Am. Meteorol. Soc.*, 82, pp. 2415–2434.
- Baldocchi, D., Penuelas, J., 2019. The physics and ecology of mining carbon dioxide from the atmosphere by ecosystems. *Global Change Biol.* 25, 1191–1197.
- Baldocchi, D.D., Ryu, Y., Dechant, B., Eichelmann, E., Hemes, K., Ma, S., Sanchez, C.R., Shortt, R., Szutu, D., Valach, A., Verfaillie, J., Badgley, G., Zeng, Y., Berry, J.A., 2020. Outgoing Near-Infrared Radiation From Vegetation Scales With Canopy

- Photosynthesis Across a Spectrum of Function, Structure, Physiological Capacity, and Weather. *J. Geophys. Res.-Biogeosci.* 125.
- Ber, C., Reichstein, M., Tomelleri, E., Ciais, P., Jung, M., Carvalhais, N., Roedenbeck, C., Arain, M.A., Baldocchi, D., Bonan, G.B., Bondeau, A., Cescatti, A., Lasslop, G., Lindroth, A., Lomas, M., Luyssaert, S., Margolis, H., Oleson, K.W., Rouspár, O., Veenendaal, E., Viovy, N., Williams, C., Woodward, F.I., Papale, D., 2010. Terrestrial gross carbon dioxide uptake: global distribution and covariation with climate. *Science* 329, 834–838.
- Cai, W., Yuan, W., Liang, S., Liu, S., Dong, W., Chen, Y., Liu, D., Zhang, H., 2014a. Large Differences in Terrestrial Vegetation Production Derived from Satellite-Based Light Use Efficiency Models. *Remote Sens.* 6, 8945–8965.
- Cai, W., Yuan, W., Liang, S., Zhang, X., Dong, W., Xia, J., Fu, Y., Chen, Y., Liu, D., Zhang, Q., 2014b. Improved estimations of gross primary production using satellite-derived photosynthetically active radiation. *J. Geophys. Res.-Biogeosci.* 119, 110–123.
- Camps-Valls, G., Campos-Taberner, M., Moreno-Martínez, Á., Walther, S., Duveiller, G., Cescatti, A., Mahecha, M.D., Muñoz-Marí, J., García-Haro, F.J., Guanter, L., Jung, M., Gamon, J.A., Reichstein, M., Running, S.W., 2021. A unified vegetation index for quantifying the terrestrial biosphere. In: *Sci. Adv.*, 7 eabc7447.
- Canadell, J., Jackson, R.B., Ehleringer, J.R., Mooney, H.A., Sala, O.E., Schulze, E.D., 1996. Maximum rooting depth of vegetation types at the global scale. *Oecologia* 108, 583–595.
- Churkina, G., Running, S.W., Schloss, A.L., Participants Potsdam, N.P.P.M.I., 1999. Comparing global models of terrestrial net primary productivity (NPP): the importance of water availability. *Global Change Biol.* 5, 46–55.
- Collatz, G.J., Ball, J.T., Grivet, C., Berry, J.A., 1991. Physiological and environmental regulation of stomatal conductance, photosynthesis and transpiration - a model that includes a laminar boundary-layer. *Agric. For. Meteorol.* 54, 107–136.
- Croft, H., Chen, J.M., Wang, R., Mo, G., Luo, S., Luo, X., He, L., Gonsamo, A., Arabian, J., Zhang, Y., Simic-Milas, A., Noland, T.L., He, Y., Homolova, L., Malenovsky, Z., Yi, Q., Beringer, J., Amiri, R., Hutley, L., Arellano, P., Stahl, C., Bonal, D., 2020. The global distribution of leaf chlorophyll content. *Remote Sens. Environ.* 236.
- Cui, T., Sun, R., Qiao, C., 2016a. Assessing the factors determining the relationship between solar-induced chlorophyll fluorescence and GPP. In: *2016 IEEE International Geoscience and Remote Sensing Symposium*, pp. 3520–3523.
- Cui, T., Wang, Y., Sun, R., Qiao, C., Fan, W., Jiang, G., Hao, L., Zhang, L., 2016b. Estimating vegetation primary production in the Heihe river basin of China with multi-source and multi-scale data. In: *PLoS One*, 11.
- Damm, A., Guanter, L., Paul-Limoges, E., van der Tol, C., Hueni, A., Buchmann, N., Eugster, W., Ammann, C., Schaepman, M.E., 2015. Far-red sun-induced chlorophyll fluorescence shows ecosystem-specific relationships to gross primary production: an assessment based on observational and modeling approaches. *Remote Sens. Environ.* 166, 91–105.
- de Almeida, C.T., Delgado, R.C., Galvao, L.S., de Oliveira Cruz e Aragão, L.E., Concepcion Ramos, M., 2018. Improvements of the MODIS Gross Primary Productivity model based on a comprehensive uncertainty assessment over the Brazilian Amazonia. *ISPRS J. Photogramm. Remote Sens.* 145, 268–283.
- Dechant, B., Ryu, Y., Badgley, G., Köhler, P., Rascher, U., Migliavacca, M., Zhang, Y., Tagliabue, G., Guan, K., Rossini, M., Goulas, Y., Zeng, Y., Frankenberg, C., Berry, J. A., 2022. NIRVP: a robust statistical proxy for sun-induced chlorophyll fluorescence and photosynthesis across scales. *Remote Sens. Environ.* 268, 112763.
- Doerken, V.M., Lepetit, B., 2018. Morpho-anatomical and physiological differences between sun and shade leaves in *Abies alba* MILL. (Pinaceae, Coniferales): a combined approach. *Plant Cell Environ.* 41, 1683–1697.
- Dong, J., Xiao, X., Wagle, P., Zhang, G., Zhou, Y., Jin, C., Torn, M.S., Meyers, T.P., Suyker, A.E., Wang, J., Yan, H., Biradar, C., Moore III, B., 2015. Comparison of four EVI-based models for estimating gross primary production of maize and soybean croplands and tallgrass prairie under severe drought. *Remote Sens. Environ.* 162, 154–168.
- Donohue, R.J., Hume, I.H., Roderick, M.L., McVicar, T.R., Beringer, J., Hutley, L., Gallant, J.C., Austin, J.M., van Gorsel, E., Cleverly, J.R., Meyer, W.S., Arndt, S.K., 2014. Evaluation of the remote-sensing-based DIFFUSE model for estimating photosynthesis of vegetation. *Remote Sens. Environ.* 155, 349–365.
- Doughty, R., Xiao, X., Köhler, P., Frankenberg, C., Qin, Y., Wu, X., Ma, S., Moore III, B., 2021. Global-Scale Consistency of Spaceborne Vegetation Indices, Chlorophyll Fluorescence, and Photosynthesis. *J. Geophys. Res.* 126 e2020JG006136.
- Drolet, G.G., Huemmrich, K.F., Hall, F.G., Middleton, E.M., Black, T.A., Barr, A.G., Margolis, H.A., 2005. A MODIS-derived photochemical reflectance index to detect inter-annual variations in the photosynthetic light-use efficiency of a boreal deciduous forest. *Remote Sens. Environ.* 98, 212–224.
- Drolet, G.G., Middleton, E.M., Huemmrich, K.F., Hall, F.G., Amiro, B.D., Barr, A.G., Black, T.A., McCaughey, J.H., Margolis, H.A., 2008. Regional mapping of gross light-use efficiency using MODIS spectral indices. *Remote Sens. Environ.* 112, 3064–3078.
- Duveiller, G., Cescatti, A., 2016. Spatially downscaling sun-induced chlorophyll fluorescence leads to an improved temporal correlation with gross primary productivity. *Remote Sens. Environ.* 182, 72–89.
- Farquhar, G.D., Caemmerer, S.V., Berry, J.A., 1980. A Biochemical-model of photosynthetic CO<sub>2</sub> assimilation in leaves of C-3 species. *Planta* 149, 78–90.
- Filella, I., Porcar-Castell, A., Munne-Bosch, S., Back, J., Garbulsky, M.F., Penuelas, J., 2009. PRI assessment of long-term changes in carotenoids/chlorophyll ratio and short-term changes in de-epoxidation state of the xanthophyll cycle. *Int. J. Remote Sens.* 30, 4443–4455.
- Frankenberg, C., Fisher, J.B., Worden, J., Badgley, G., Saatchi, S.S., Lee, J.-E., Toon, G.C., Butz, A., Jung, M., Kuze, A., Yokota, T., 2011. New global observations of the terrestrial carbon cycle from GOSAT: patterns of plant fluorescence with gross primary productivity. *Geophys. Res. Lett.* 38.
- Gamon, J.A., Berry, J.A., 2012. Facultative and constitutive pigment effects on the Photochemical Reflectance Index (PRI) in sun and shade conifer needles. *Israel J. Plant Sci.* 60, 85–95.
- Gamon, J.A., Penuelas, J., Field, C.B., 1992. A narrow-waveband spectral index that tracks diurnal changes in photosynthetic efficiency. *Remote Sens. Environ.* 41, 35–44.
- Gao, Y., Yu, G., Yan, H., Zhu, X., Li, S., Wang, Q., Zhang, J., Wang, Y., Li, Y., Zhao, L., Shi, P., 2014. A MODIS-based photosynthetic capacity model to estimate gross primary production in Northern China and the Tibetan plateau. *Remote Sens. Environ.* 148, 108–118.
- Garbulsky, M.F., Penuelas, J., Gamon, J., Inoue, Y., Filella, I., 2011. The photochemical reflectance index (PRI) and the remote sensing of leaf, canopy and ecosystem radiation use efficiencies A review and meta-analysis. *Remote Sens. Environ.* 115, 281–297.
- Garbulsky, M.F., Penuelas, J., Papale, D., Ardo, J., Goulden, M.L., Kiely, G., Richardson, A.D., Rotenberg, E., Veenendaal, E.M., Filella, I., 2010. Patterns and controls of the variability of radiation use efficiency and primary productivity across terrestrial ecosystems. *Global Ecol. Biogeogr.* 19, 253–267.
- Garbulsky, M.F., Penuelas, J., Papale, D., Filella, I., 2008. Remote estimation of carbon dioxide uptake by a Mediterranean forest. *Global Change Biol.* 14, 2860–2867.
- Giri, C., Zhu, Z.L., Reed, B., 2005. A comparative analysis of the Global Land Cover 2000 and MODIS land cover data sets. *Remote Sens. Environ.* 94, 123–132.
- Gitelson, A.A., Gamon, J.A., 2015. The need for a common basis for defining light-use efficiency: implications for productivity estimation. *Remote Sens. Environ.* 156, 196–201.
- Gitelson, A.A., Vina, A., Verma, S.B., Rundquist, D.C., Arkebauer, T.J., Keydan, G., Leavitt, B., Ciganda, V., Burba, G.G., Suyker, A.E., 2006. Relationship between gross primary production and chlorophyll content in crops: implications for the synoptic monitoring of vegetation productivity. *J. Geophys. Res.-Atmosph.* 111.
- Goerner, A., Reichstein, M., Tomelleri, E., Hanan, N., Rambal, S., Papale, D., Dragoni, D., Schmullius, C., 2011. Remote sensing of ecosystem light use efficiency with MODIS-based PRI. *Biogeosciences* 8, 189–202.
- Guanter, L., Zhang, Y., Jung, M., Joiner, J., Voigt, M., Berry, J.A., Frankenberg, C., Huete, A.R., Zarco-Tejada, P., Lee, J.-E., Moran, M.S., Ponce-Campos, G., Beer, C., Camps-Valls, G., Buchmann, N., Gianelle, D., Klumpp, K., Cescatti, A., Baker, J.M., Griffis, T.J., 2014. Global and time-resolved monitoring of crop photosynthesis with chlorophyll fluorescence. In: *Proc. Nat. Acad. Sci. U.S.A.*, 111, pp. E1327–E1333.
- He, M., Ju, W., Zhou, Y., Chen, J., He, H., Wang, S., Wang, H., Guan, D., Yan, J., Li, Y., Hao, Y., Zhao, F., 2013. Development of a two-leaf light use efficiency model for improving the calculation of terrestrial gross primary productivity. *Agric. For. Meteorol.* 173, 28–39.
- He, M., Kimball, J.S., Running, S., Ballantyne, A., Guan, K., Huemmrich, F., 2016. Satellite detection of soil moisture related water stress impacts on ecosystem productivity using the MODIS-based photochemical reflectance index. *Remote Sens. Environ.* 186, 173–183.
- Hainsch, F.A., Zhao, M., Running, S.W., Kimball, J.S., Nemani, R.R., Davis, K.J., Bolstad, P.V., Cook, B.D., Desai, A.R., Ricciuto, D.M., Law, B.E., Oechel, W.C., Kwon, H., Luo, H., Wofsy, S.C., Dunn, A.L., Munger, J.W., Baldocchi, D.D., Xu, L., Hollinger, D.Y., Richardson, A.D., Stoy, P.C., Siqueira, M.B.S., Monson, R.K., Burns, S.P., Flanagan, L.B., 2006. Evaluation of remote sensing based terrestrial productivity from MODIS using regional tower eddy flux network observations. *IEEE Trans. Geosci. Remote Sens.* 44, 1908–1925.
- Helm, L.T., Shi, H., Lerdau, M.T., Yang, X., 2020. Solar-induced chlorophyll fluorescence and short-term photosynthetic response to drought. *Ecol. Appl.* 30, e02101.
- Hilker, T., Coops, N.C., Wilder, M.A., Black, T.A., Guy, R.D., 2008. The use of remote sensing in light use efficiency based models of gross primary production: a review of current status and future requirements. *Sci. Total Environ.* 404, 411–423.
- Hilker, T., Lyapustin, A., Hall, F.G., Wang, Y., Coops, N.C., Drolet, G., Black, T.A., 2009. An assessment of photosynthetic light use efficiency from space: modeling the atmospheric and directional impacts on PRI reflectance. *Remote Sens. Environ.* 113, 2463–2475.
- Huete, A., Didan, K., Miura, T., Rodriguez, E.P., Gao, X., Ferreira, L.G., 2002. Overview of the radiometric and biophysical performance of the MODIS vegetation indices. *Remote Sens. Environ.* 83, 195–213.
- Huete, A.R., Liu, H.Q., vanLeeuwen, W.J.D., & Ieee (1997). *The use of vegetation indices in forested regions: issues of linearity and saturation*.
- Jiang, C., Ryu, Y., 2016. Multi-scale evaluation of global gross primary productivity and evapotranspiration products derived from Breathing Earth System Simulator (BESS). *Remote Sens. Environ.* 186, 528–547.
- Jung, M., Reichstein, M., Bondeau, A., 2009. Towards global empirical upscaling of FLUXNET eddy covariance observations: validation of a model tree ensemble approach using a biosphere model. *Biogeosciences* 6, 2001–2013.
- Jung, M., Reichstein, M., Margolis, H.A., Cescatti, A., Richardson, A.D., Arain, M.A., Arneth, A., Bernhofer, C., Bonal, D., Chen, J., Gianelle, D., Gobron, N., Kiely, G., Kutsch, W., Lasslop, G., Law, B.E., Lindroth, A., Merbold, L., Montagnani, L., Moors, E.J., Papale, D., Sottocornola, M., Vaccari, F., Williams, C., 2011. Global patterns of land-atmosphere fluxes of carbon dioxide, latent heat, and sensible heat derived from eddy covariance, satellite, and meteorological observations. *J. Geophys. Res.-Biogeosci.* 116.
- Jung, M., Schwalm, C., Migliavacca, M., Walther, S., Camps-Valls, G., Koiralala, S., Anthoni, P., Besnard, S., Bodesheim, P., Carvalhais, N., Chevallier, F., Gans, F., Goll, D.S., Haverd, V., Köhler, P., Ichii, K., Jain, A.K., Liu, J., Lombardozzi, D., Nabel, J.E.M.S., Nelson, J.A., O'Sullivan, M., Pallandt, M., Papale, D., Peters, W., Pongratz, J., Rödenbeck, C., Sitch, S., Tramontana, G., Walker, A., Weber, U., Reichstein, M., 2020. Scaling carbon fluxes from eddy covariance sites to globe: synthesis and evaluation of the FLUXCOM approach. *Biogeosciences* 17, 1343–1365.

- King, D.A., Turner, D.P., Ritts, W.D., 2011. Parameterization of a diagnostic carbon cycle model for continental scale application. *Remote Sens. Environ.* 115, 1653–1664.
- Klein, T., Yakir, D., Buchmann, N., Gruenewig, J.M., 2014. Towards an advanced assessment of the hydrological vulnerability of forests to climate change-induced drought. *New Phytol.* 201, 712–716.
- Landsberg, J.J., Waring, R.H., 1997. A generalised model of forest productivity using simplified concepts of radiation-use efficiency, carbon balance and partitioning. *Forest Ecol. Manag.* 95, 209–228.
- Le Quere, C., Andrew, R.M., Canadell, J.G., Sitch, S., Korsbakken, J.I., Peters, G.P., Manning, A.C., Boden, T.A., Tans, P.P., Houghton, R.A., Keeling, R.F., Alin, S., Andrews, O.D., Anthoni, P., Barbero, L., Bopp, L., Chevallier, F., Chini, L.P., Ciais, P., Currie, K., Delire, C., Doney, S.C., Friedlingstein, P., Gkritzalis, T., Harris, I., Hauck, J., Haverd, V., Hoppema, M., Goldewijk, K.K., Jain, A.K., Kato, E., Kortzinger, A., Landschutzer, P., Lefevre, N., Lenton, A., Lienert, S., Lombardozzi, D., Melton, J.R., Metzl, N., Millero, F., Monteiro, P.M.S., Munro, D.R., Nabel, J., Nakaoka, S., O'Brien, K., Olsen, A., Omar, A.M., Ono, T., Pierrot, D., Poulet, B., Reddenbeck, C., Salisbury, J., Schuster, U., Schwinger, J., Seferian, R., Skjelvan, I., Stocker, B.D., Sutton, A.J., Takahashi, T., Tian, H.Q., Tilbrook, B., van der Laan-Luijkx, I.T., van der Werf, G.R., Viovy, N., Walker, A.P., Wiltshire, A.J., Zaehle, S., 2016. Global carbon budget 2016. *Earth Syst. Sci. Data* 8, 605–649.
- Lees, K.J., Quaife, T., Artz, R.R.E., Khomik, M., Clark, J.M., 2018. Potential for using remote sensing to estimate carbon fluxes across northern peatlands - a review. *Sci. Total Environ.* 615, 857–874.
- Leuning, R., Cleugh, H.A., Zegelin, S.J., Hughes, D., 2005. Carbon and water fluxes over a temperate Eucalyptus forest and a tropical wet/dry savanna in Australia: measurements and comparison with MODIS remote sensing estimates. *Agric. For. Meteorol.* 129, 151–173.
- Li, X., Xiao, J., 2019. Mapping photosynthesis solely from solar-induced chlorophyll fluorescence: a global, fine-resolution dataset of gross primary production derived from OCO-2. *Remote Sens.* 11.
- Li, X., Xiao, J., He, B., 2018a. Chlorophyll fluorescence observed by OCO-2 is strongly related to gross primary productivity estimated from flux towers in temperate forests. *Remote Sens. Environ.* 204, 659–671.
- Li, X., Xiao, J., He, B., Arain, M.A., Beringer, J., Desai, A.R., Emmel, C., Hollinger, D.Y., Krasnova, A., Mammarella, I., Noe, S.M., Serrano Ortiz, P., Rey-Sanchez, A.C., Rocha, A.V., Varlagin, A., 2018b. Solar-induced chlorophyll fluorescence is strongly correlated with terrestrial photosynthesis for a wide variety of biomes: first global analysis based on OCO-2 and flux tower observations. *Global Change Biol.* 24, 3990–4008.
- Lichtenthaler, H.K., Buschmann, C., Doll, M., Fietz, H.J., Bach, T., Kozel, U., Meier, D., Rahmsdorf, U., 1981. Photosynthetic activity, chloroplast ultrastructure, and leaf characteristics of high-light and low-light plants and of sun and shade leaves. *Photosynth. Res.* 2, 115–141.
- Madani, N., Kimball, J.S., Affleck, D.L.R., Kattge, J., Graham, J., van Bodegom, P.M., Reich, P.B., Running, S.W., 2014. Improving ecosystem productivity modeling through spatially explicit estimation of optimal light use efficiency. *J. Geophys. Res.-Biogeosci.* 119, 1755–1769.
- Magnay, T.S., Barnes, M.L., Yang, X., 2020a. On the covariation of chlorophyll fluorescence and photosynthesis across scales. *Geophys. Res. Lett.* 47.
- Magnay, T.S., Barnes, M.L., Yang, X., 2020b. On the covariation of chlorophyll fluorescence and photosynthesis across scales. *Geophys. Res. Lett.* 47, e2020GL091098.
- Marques Caldeira, D.R., Alvares, C.A., Campoe, O.C., Hakamada, R.E., Guerrini, I.A., Cegatta, I.R., Stape, J.L., 2020. Multisite evaluation of the 3-PG model for the highest phenotypic plasticity Eucalyptus clone in Brazil. *Forest Ecol. Manag.* 462.
- Marrs, J.K., Reblin, J.S., Logan, B.A., Allen, D.W., Reinmann, A.B., Bombard, D.M., Tabachnik, D., Hutyra, L.R., 2020. Solar-induced fluorescence does not track photosynthetic carbon assimilation following induced stomatal closure. *Geophys. Res. Lett.* 47, e2020GL087975.
- Monteith, J.L., 1972. Solar-radiation and productivity in tropical ecosystems. *J. Appl. Ecol.* 9, 747–766.
- Moreno, A., Masetti, F., Gilabert, M.A., Chiesi, M., Martinez, B., Seufert, G., 2012. Assessment of MODIS imagery to track light-use efficiency in a water-limited Mediterranean pine forest. *Remote Sens. Environ.* 123, 359–367.
- Myinen, R.B., Los, S.O., Asrar, G., 1995. Potential gross primary productivity of terrestrial vegetation from 1982–1990. *Geophys. Res. Lett.* 22, 2617–2620.
- Ocheltree, T.W., Nippert, J.B., Prasad, P.V.V., 2014. Stomatal responses to changes in vapor pressure deficit reflect tissue-specific differences in hydraulic conductance. *Plant Cell Environ.* 37, 132–139.
- Penuelas, J., Garbulsky, M.F., Filella, I., 2011. Photochemical reflectance index (PRI) and remote sensing of plant CO<sub>2</sub> uptake. *New Phytol.* 191, 596–599.
- Perez-Priego, O., Guan, J., Rossini, M., Fava, F., Wutzler, T., Moreno, G., Carvalhais, N., Carrara, A., Kolle, O., Julitta, T., Schrumpf, M., Reichstein, M., Migliavacca, M., 2015. Sun-induced chlorophyll fluorescence and photochemical reflectance index improve remote-sensing gross primary production estimates under varying nutrient availability in a typical Mediterranean savanna ecosystem. *Biogeosciences* 12, 6351–6367.
- Potter, C.S., Randerson, J.T., Field, C.B., Matson, P.A., Vitousek, P.M., Mooney, H.A., Klooster, S.A., 1993. Terrestrial ecosystem production - a process model-based on global satellite and surface data. *Global Biogeochem. Cycles* 7, 811–841.
- Prince, S.D., Goward, S.N., 1995. Global primary production: a remote sensing approach. *J. Biogeogr.* 22, 815–835.
- Reichle, R.H., Liu, Q., Koster, R.D., Crow, W., De Lannoy, G.J.M., Kimball, J.S., Ardizzone, J.V., Bosch, D., Colliander, A., Cosh, M., Kolassa, J., Mahanama, S.P., Prueger, J., Starks, P., Walker, J.P., 2019. Version 4 of the SMAP Level-4 soil moisture algorithm and data product. *J. Adv. Model. Earth Syst.* 11, 3106–3130.
- Reichstein, M., Falge, E., Baldocchi, D., Papale, D., Aubinet, M., Berbigier, P., Bernhofer, C., Buchmann, N., Gilmanov, T., Granier, A., Grunwald, T., Havrankova, K., Ilvesniemi, H., Janous, D., Knoblauch, A., Laurila, T., Lohila, A., Loustau, D., Matteucci, G., Meyers, T., Miglietta, F., Ourcival, J.M., Pumpanen, J., Rambal, S., Rotenberg, E., Sanz, M., Tenhunen, J., Seufert, G., Vaccari, F., Vesala, T., Yakir, D., Valentini, R., 2005. On the separation of net ecosystem exchange into assimilation and ecosystem respiration: review and improved algorithm. *Global Change Biol.* 11, 1424–1439.
- Reyer, C.P.O., Leuzinger, S., Rammig, A., Wolf, A., Bartholomeus, R.P., Bonfante, A., de Lorenzi, F., Dury, M., Gloning, P., Abou Jaoude, R., Klein, T., Kuster, T.M., Martins, M., Niedrist, G., Riccardi, M., Wohlfahrt, G., de Angelis, P., de Dato, G., Francois, L., Menzel, A., Pereira, M., 2013. A plant's perspective of extremes: terrestrial plant responses to changing climatic variability. *Global Change Biol.* 19, 75–89.
- Ruimy, A., Kergoat, L., Bondeau, A., Participants Potsdam, N.P.P.M.I., 1999. Comparing global models of terrestrial net primary productivity (NPP): analysis of differences in light absorption and light-use efficiency. *Global Change Biol.* 5, 56–64.
- Ruimy, A., Saugier, B., Dedieu, G., 1994. Methodology for the estimation of terrestrial net primary production from remotely sensed data. *J. Geophys. Res.-Atmos.* 99, 5263–5283.
- Running, S.W., Nemani, R.R., Heinsch, F.A., Zhao, M.S., Reeves, M., Hashimoto, H., 2004. A continuous satellite-derived measure of global terrestrial primary production. *Bioscience* 54, 547–560.
- Running, S.W., Thornton, P.E., Nemani, R., Glassy, J.M., 2000. Global terrestrial gross and net primary productivity from the earth observing system. *Method. Ecosyst. Sci.* 44–57.
- Ryu, Y., Baldocchi, D.D., Kobayashi, H., van Ingen, C., Li, J., Black, T.A., Beringer, J., van Gorsel, E., Knoblauch, A., Law, B.E., Roupard, O., 2011. Integration of MODIS land and atmosphere products with a coupled-process model to estimate gross primary productivity and evapotranspiration from 1 km to global scales. *Global Biogeochem. Cycles* 25.
- Ryu, Y., Berry, J.A., Baldocchi, D.D., 2019. What is global photosynthesis? History, uncertainties and opportunities. *Remote Sens. Environ.* 223, 95–114.
- Ryu, Y., Jiang, C., Kobayashi, H., Dettò, M., 2018. MODIS-derived global land products of shortwave radiation and diffuse and total photosynthetically active radiation at 5 km resolution from 2000. *Remote Sens. Environ.* 204, 812–825.
- Schaefer, K., Schwalm, C.R., Williams, C., Arain, M.A., Barr, A., Chen, J.M., Davis, K.J., Dimitrov, D., Hilton, T.W., Hollinger, D.Y., Humphreys, E., Poulter, B., Racine, B.M., Richardson, A.D., Sahoo, A., Thornton, P., Vargas, R., Verbeeck, H., Anderson, R., Baker, I., Black, T.A., Bolstad, P., Chen, J., Curtis, P.S., Desai, A.R., Dietze, M., Dragoni, D., Gough, C., Grant, R.F., Gu, L., Jain, A., Kucharik, C., Law, B., Liu, S., Lokipitiya, E., Margolis, H.A., Matamala, R., McCaughey, J.H., Monson, R., Munger, J.W., Oechel, W., Peng, C., Price, D.T., Ricciuto, D., Riley, W.J., Roulet, N., Tian, H., Tonitto, C., Torn, M., Weng, E., & Zhou, X. (2012). A model-data comparison of gross primary productivity: results from the North American Carbon Program site synthesis. *J. Geophys. Res.-Biogeosci.*, 117.
- Schenk, H.J., Jackson, R.B., 2002. The global biogeography of roots. *Ecol. Monographs* 72, 311–328.
- Serbin, S.P., Ahl, D.E., Gower, S.T., 2013. Spatial and temporal validation of the MODIS LAI and FPAR products across a boreal forest wildfire chronosequence. *Remote Sens. Environ.* 133, 71–84.
- Shangguan, W., Dai, Y., Duan, Q., Liu, B., Yuan, H., 2014. A global soil data set for earth system modeling. *J. Adv. Model. Earth Syst.* 6, 249–263.
- Sheffield, J., Goteti, G., Wood, E.F., 2006. Development of a 50-year high-resolution global dataset of meteorological forcings for land surface modeling. *J. Climate* 19, 3088–3111.
- Sims, D.A., Brzostek, E.R., Rahman, A.F., Dragoni, D., Phillips, R.P., 2014. An improved approach for remotely sensing water stress impacts on forest C uptake. *Global Change Biol.* 20, 2856–2866.
- Stagakis, S., Markos, N., Sykioti, O., Kyparissis, A., 2014. Tracking seasonal changes of leaf and canopy light use efficiency in a *Phlomis fruticosa* Mediterranean ecosystem using field measurements and multi-angular satellite hyperspectral imagery. *ISPRS J. Photogramm. Remote Sens.* 97, 138–151.
- Stocker, B.D., Zscheischler, J., Keenan, T.F., Prentice, I.C., Peñuelas, J., Seneviratne, S.I., 2018. Quantifying soil moisture impacts on light use efficiency across biomes. *New Phytol.* 218, 1430–1449.
- Stocker, B.D., Zscheischler, J., Keenan, T.F., Prentice, I.C., Seneviratne, S.I., Peñuelas, J., 2019. Drought impacts on terrestrial primary production underestimated by satellite monitoring. *Nat. Geosci.* 12, 264. -.
- Sun, R., Zhu, Q., 1999. Net primary productivity of terrestrial vegetation - a review on related researches. *Chinese J. Appl. Ecol.* 10 (757), 760.
- Tramontana, G., Jung, M., Schwalm, C.R., Ichii, K., Camps-Valls, G., Raduly, B., Reichstein, M., Arain, M.A., Cescatti, A., Kiely, G., Merbold, L., Serrano-Ortiz, P., Sickert, S., Wolf, S., Papale, D., 2016. Predicting carbon dioxide and energy fluxes across global FLUXNET sites with regression algorithms. *Biogeosciences* 13, 4291–4313.
- Turner, D.P., Ritts, W.D., Cohen, W.B., Gower, S.T., Zhao, M.S., Running, S.W., Wofsy, S. C., Urbanski, S., Dunn, A.L., Munger, J.W., 2003. Scaling Gross Primary Production (GPP) over boreal and deciduous forest landscapes in support of MODIS GPP product validation. *Remote Sens. Environ.* 88, 256–270.
- Turner, D.P., Ritts, W.D., Styles, J.M., Yang, Z., Cohen, W.B., Law, B.E., Thornton, P.E., 2006. A diagnostic carbon flux model to monitor the effects of disturbance and interannual variation in climate on regional NEP. *Tellus Series B-Chem. Phys. Meteorol.* 58, 476–490.

- Turner, D.P., Ritts, W.D., Wharton, S., Thomas, C., Monson, R., Black, T.A., Falk, M., 2009. Assessing FPAR source and parameter optimization scheme in application of a diagnostic carbon flux model. *Remote Sens. Environ.* 113, 1529–1539.
- Veroustraete, F., Sabbe, H., Eerens, H., 2002. Estimation of carbon mass fluxes over Europe using the C-Fix model and Euroflux data. *Remote Sens. Environ.* 83, 376–399.
- Wagle, P., Gowda, P.H., Xiao, X., Anup, K.C., 2016. Parameterizing ecosystem light use efficiency and water use efficiency to estimate maize gross primary production and evapotranspiration using MODIS EVI. *Agric. For. Meteorol.* 222, 87–97.
- Walker, J.J., de Beurs, K.M., Wynne, R.H., 2014. Dryland vegetation phenology across an elevation gradient in Arizona, USA, investigated with fused MODIS and Landsat data. *Remote Sens. Environ.* 144, 85–97.
- Wang, L., Zhu, H., Lin, A., Zou, L., Qin, W., Du, Q., 2017. Evaluation of the latest MODIS GPP products across multiple biomes using global eddy covariance flux data. *Remote Sensing* 9.
- Wang, S., Huang, K., Yan, H., Yan, H., Zhou, L., Wang, H., Zhang, J., Yan, J., Zhao, L., Wang, Y., Shi, P., Zhao, F., Sun, L., 2015. Improving the light use efficiency model for simulating terrestrial vegetation gross primary production by the inclusion of diffuse radiation across ecosystems in China. *Ecol. Complex.* 23, 1–13.
- Wang, S., Iacob, A., Bauer-Gottwein, P., Garcia, M., 2018. Incorporating diffuse radiation into a light use efficiency and evapotranspiration model: an 11-year study in a high latitude deciduous forest. *Agric. For. Meteorol.* 248, 479–493.
- Wang, S., Zhang, Y., Ju, W., Qiu, B., Zhang, Z., 2021. Tracking the seasonal and inter-annual variations of global gross primary production during last four decades using satellite near-infrared reflectance data. *Sci. Total Environ.* 755.
- Wang, X., Chen, J.M., Ju, W., 2020. Photochemical reflectance index (PRI) can be used to improve the relationship between gross primary productivity (GPP) and sun-induced chlorophyll fluorescence (SIF). *Remote Sens. Environ.* 246, 11188.
- Welp, L.R., Keeling, R.F., Meijer, H.A.J., Bollenbacher, A.F., Piper, S.C., Yoshimura, K., Francey, R.J., Allison, C.E., Wahlen, M., 2011. Interannual variability in the oxygen isotopes of atmospheric CO<sub>2</sub> driven by El Niño. *Nature* 477, 579–582.
- Wu, C., Chen, J.M., Desai, A.R., Hollinger, D.Y., Arain, M.A., Margolis, H.A., Gough, C.M., Staebler, R.M., 2012. Remote sensing of canopy light use efficiency in temperate and boreal forests of North America using MODIS imagery. *Remote Sens. Environ.* 118, 60–72.
- Wu, C., Munger, J.W., Niu, Z., Kuang, D., 2010. Comparison of multiple models for estimating gross primary production using MODIS and eddy covariance data in Harvard Forest. *Remote Sens. Environ.* 114, 2925–2939.
- Wu, G., Guan, K., Jiang, C., Peng, B., Kimm, H., Chen, M., Yang, X., Wang, S., Suyker, A.E., Bernacchi, C.J., Moore, C.E., Zeng, Y., Berry, J.A., Pilar Cendrero-Mateo, M., 2020. Radiance-based NIRv as a proxy for GPP of corn and soybean. *Environ. Res. Lett.* 15.
- Wu, X., Ju, W., Zhou, Y., He, M., Law, B.E., Black, T.A., Margolis, H.A., Cescatti, A., Gu, L., Montagnani, L., Noormets, A., Griffis, T.J., Pilegaard, K., Varlagin, A., Valentini, R., Blanken, P.D., Wang, S., Wang, H., Han, S., Yan, J., Li, Y., Zhou, B., Liu, Y., 2015. Performance of linear and nonlinear two-leaf light use efficiency models at different temporal scales. *Remote Sens.* 7, 2238–2278.
- Xia, J., Niu, S., Ciais, P., Janssens, I.A., Chen, J., Ammann, C., Arain, A., Blanken, P.D., Cescatti, A., Bonal, D., Buchmann, N., Curtis, P.S., Chen, S., Dong, J., Flanagan, L.B., Frankenberg, C., Georgiadis, T., Gough, C.M., Hui, D., Kiely, G., Li, J., Lund, M., Magliulo, V., Marcolla, B., Merbold, L., Montagnani, L., Moors, E.J., Olesen, J.E., Piao, S., Raschi, A., Rousard, O., Suyker, A.E., Urbaniak, M., Vaccari, F.P., Varlagin, A., Vesala, T., Wilkinson, M., Weng, E., Wohlfahrt, G., Yan, L., Luo, Y., 2015. Joint control of terrestrial gross primary productivity by plant phenology and physiology. In: *Proc. Nat. Acad. Sci. U.S.A.*, 112, pp. 2788–2793.
- Xiao, J., Davis, K.J., Urban, N.M., Keller, K., 2014. Uncertainty in model parameters and regional carbon fluxes: a model-data fusion approach. *Agric. For. Meteorol.* 189, 175–186.
- Xiao, J., Zhuang, Q., Law, B.E., Chen, J., Baldocchi, D.D., Cook, D.R., Oren, R., Richardson, A.D., Wharton, S., Ma, S., Martin, T.A., Verma, S.B., Suyker, A.E., Scott, R.L., Monson, R.K., Litvak, M., Hollinger, D.Y., Sun, G., Davis, K.J., Bolstad, P.V., Burns, S.P., Curtis, P.S., Drake, B.G., Falk, M., Fischer, M.L., Foster, D.R., Gu, L., Hadley, J.L., Katul, G.G., Matamala, R., McNulty, S., Meyers, T.P., Munger, J.W., Noormets, A., Oechel, W.C., Paw, U.K.T., Schmid, H.P., Starr, G., Torn, M.S., Wofsy, S.C., 2010. A continuous measure of gross primary production for the conterminous United States derived from MODIS and AmeriFlux data. *Remote Sens. Environ.* 114, 576–591.
- Xiao, X.M., Hollinger, D., Aber, J., Goltz, M., Davidson, E.A., Zhang, Q.Y., Moore, B., 2004a. Satellite-based modeling of gross primary production in an evergreen needleleaf forest. *Remote Sens. Environ.* 89, 519–534.
- Xiao, X.M., Zhang, Q.Y., Braswell, B., Urbanski, S., Boles, S., Wofsy, S., Berrien, M., Ojima, D., 2004b. Modeling gross primary production of temperate deciduous broadleaf forest using satellite images and climate data. *Remote Sens. Environ.* 91, 256–270.
- Xiao, Z., Liang, S., Wang, T., Jiang, B., 2016. Retrieval of leaf area Index (LAI) and fraction of absorbed photosynthetically active radiation (FAPAR) from VIIRS time-series data. *Remote Sens.* 8.
- Yan, H., Wang, S.-q., Billesbach, D., Oechel, W., Bohrer, G., Meyers, T., Martin, T.A., Matamala, R., Phillips, R.P., Rahman, F., Yu, Q., Shugart, H.H., 2015. Improved global simulations of gross primary product based on a new definition of water stress factor and a separate treatment of C3 and C4 plants. *Ecol. Modell.* 297, 42–59.
- Yan, H., Wang, S.-Q., da Rocha, H.R., Rap, A., Bonal, D., Butt, N., Coupe, N.R., Shugart, H.H., 2017a. Simulation of the unexpected photosynthetic seasonality in amazonian evergreen forests by using an improved diffuse fraction-based light use efficiency model. *J. Geophys. Res.-Biogeosci.* 122, 3014–3030.
- Yan, H., Wang, S.-Q., Yu, K.-L., Wang, B., Yu, Q., Bohrer, G., Billesbach, D., Bracho, R., Rahman, F., Shugart, H.H., 2017b. A novel diffuse fraction-based two-leaf light use efficiency model: an application quantifying photosynthetic seasonality across 20 AmeriFlux flux tower sites. *J. Adv. Model. Earth Syst.* 9, 2317–2332.
- Yang, F., Ichii, K., White, M.A., Hashimoto, H., Michaelis, A.R., Votava, P., Zhu, A.X., Huete, A., Running, S.W., Nemani, R.R., 2007. Developing a continental-scale measure of gross primary production by combining MODIS and AmeriFlux data through Support Vector Machine approach. *Remote Sens. Environ.* 110, 109–122.
- Yang, X., Tang, J., Mustard, J.F., Lee, J.-E., Rossini, M., Joiner, J., Munger, J.W., Kornfeld, A., Richardson, A.D., 2015. Solar-induced chlorophyll fluorescence that correlates with canopy photosynthesis on diurnal and seasonal scales in a temperate deciduous forest. *Geophys. Res. Lett.* 42, 2977–2987.
- Yebra, M., Van Dijk, A.J.M., Leuning, R., Guerschman, J.P., 2015. Global vegetation gross primary production estimation using satellite-derived light-use efficiency and canopy conductance. *Remote Sens. Environ.* 163, 206–216.
- Yi, Y., Kimball, J.S., Jones, L.A., Reichle, R.H., Nemani, R., Margolis, H.A., 2013. Recent climate and fire disturbance impacts on boreal and arctic ecosystem productivity estimated using a satellite-based terrestrial carbon flux model. *J. Geophys. Res.-Biogeosci.* 118, 606–622.
- Yuan, W., Cai, W., Xia, J., Chen, J., Liu, S., Dong, W., Merbold, L., Law, B., Arain, A., Beringer, J., Bernhofer, C., Black, A., Blanken, P.D., Cescatti, A., Chen, Y., Francois, L., Gianelle, D., Janssens, I.A., Jung, M., Kato, T., Kiely, G., Liu, D., Marcolla, B., Montagnani, L., Raschi, A., Rousard, O., Varlagin, A., Wohlfahrt, G., 2014. Global comparison of light use efficiency models for simulating terrestrial vegetation gross primary production based on the La Thuile database. *Agric. For. Meteorol.* 192, 108–120.
- Yuan, W., Liu, S., Yu, G., Bonnefond, J.-M., Chen, J., Davis, K., Desai, A.R., Goldstein, A.H., Gianelle, D., Rossi, F., Suyker, A.E., Verma, S.B., 2010. Global estimates of evapotranspiration and gross primary production based on MODIS and global meteorology data. *Remote Sens. Environ.* 114, 1416–1431.
- Yuan, W., Liu, S., Zhou, G., Zhou, G., Tieszen, L.L., Baldocchi, D., Bernhofer, C., Ghosh, H., Goldstein, A.H., Goulden, M.L., Hollinger, D.Y., Hu, Y., Law, B.E., Stoy, P.C., Vesala, T., Wofsy, S.C., AmeriFlux, C., 2007. Deriving a light use efficiency model from eddy covariance flux data for predicting daily gross primary production across biomes. *Agric. For. Meteorol.* 143, 189–207.
- Yuan, W., Zheng, Y., Piao, S., Ciais, P., Lombardozzi, D., Wang, Y., Ryu, Y., Chen, G., Dong, W., Hu, Z., Jain, A.K., Jiang, C., Kato, E., Li, S., Lienert, S., Liu, S., Nabel, J.E.M.S., Qin, Z., Quine, T., Sitch, S., Smith, W.K., Wang, F., Wu, C., Xiao, Z., and Yang, S., 2019. Increased atmospheric vapor pressure deficit reduces global vegetation growth. *Sci. Adv.*, 5.
- Zhang, L.-X., Zhou, D.-C., Fan, J.-W., Hu, Z.-M., 2015a. Comparison of four light use efficiency models for estimating terrestrial gross primary production. *Ecol. Model.* 300, 30–39.
- Zhang, L., Zhou, D., Fan, J., Guo, Q., Chen, S., Wang, R., Li, Y., 2019a. Contrasting the Performance of Eight Satellite-Based GPP Models in Water-Limited and Temperature-Limited Grassland Ecosystems. *Remote Sens.* 11.
- Zhang, Q., Xiao, X., Braswell, B., Linder, E., Baret, F., Moore, B., 2005. Estimating light absorption by chlorophyll, leaf and canopy in a deciduous broadleaf forest using MODIS data and a radiative transfer model. *Remote Sens. Environ.* 99, 357–371.
- Zhang, Q., Xiao, X., Braswell, B., Linder, E., Ollinger, S., Smith, M.-L., Jenkins, J.P., Baret, F., Richardson, A.D., Moore, B., Minocha, R., 2006. Characterization of seasonal variation of forest canopy in a temperate deciduous broadleaf forest, using daily MODIS data. *Remote Sens. Environ.* 105, 189–203.
- Zhang, Y., Guanter, L., Berry, J.A., van der Tol, C., Yang, X., Tang, J., Zhang, F., 2016a. Model-based analysis of the relationship between sun-induced chlorophyll fluorescence and gross primary production for remote sensing applications. *Remote Sens. Environ.* 187, 145–155.
- Zhang, Y., Kong, D., Gan, R., Chiew, F.H.S., McVicar, T.R., Zhang, Q., Yang, Y., 2019b. Coupled estimation of 500 m and 8-day resolution global evapotranspiration and gross primary production in 2002–2017. *Remote Sens. Environ.* 222, 165–182.
- Zhang, Y., Parazoo, N.C., Williams, A.P., Zhou, S., Gentile, P., 2020. Large and projected strengthening moisture limitation on end-of-season photosynthesis. In: Proceedings of the National Academy of Sciences, 117, p. 9216.
- Zhang, Y., Song, C., Sun, G., Band, L.E., McNulty, S., Noormets, A., Zhang, Q., Zhang, Z., 2016b. Development of a coupled carbon and water model for estimating global gross primary productivity and evapotranspiration based on eddy flux and remote sensing data. *Agric. For. Meteorol.* 223, 116–131.
- Zhang, Y., Song, C., Sun, G., Band, L.E., Noormets, A., Zhang, Q., 2015b. Understanding moisture stress on light use efficiency across terrestrial ecosystems based on global flux and remote-sensing data. *J. Geophys. Res.-Biogeosci.* 120, 2053–2066.
- Zhang, Y., Xiao, X., Jin, C., Dong, J., Zhou, S., Wagle, P., Joiner, J., Guanter, L., Zhang, Y., Zhang, G., Qin, Y., Wang, J., Moore III, B., 2016c. Consistency between sun-induced chlorophyll fluorescence and gross primary production of vegetation in North America. *Remote Sens. Environ.* 183, 154–169.
- Zhang, Y., Xiao, X., Wolf, S., Wu, J., Wu, X., Gioli, B., Wohlfahrt, G., Cescatti, A., van der Tol, C., Zhou, S., Gough, C.M., Gentile, P., Zhang, Y., Steinbrecher, R., Ardo, J., 2018a. Spatio-Temporal Convergence of Maximum Daily Light-Use Efficiency Based on Radiation Absorption by Canopy Chlorophyll. *Geophys. Res. Lett.* 45, 3508–3519.
- Zhang, Y., Xiao, X., Wu, X., Zhou, S., Zhang, G., Qin, Y., Dong, J., 2017. Data descriptor: a global moderate resolution dataset of gross primary production of vegetation for 2000–2016. In: *Sci. Data*, 4.
- Zhang, Y., Xiao, X., Zhang, Y., Wolf, S., Zhou, S., Joiner, J., Guanter, L., Verma, M., Sun, Y., Yang, X., Paul-Limoges, E., Gough, C.M., Wohlfahrt, G., Gioli, B., van der Tol, C., Nouvellon, Y., Lund, M., de Grandcourt, A., 2018b. On the relationship between sub-daily instantaneous and daily total gross primary production:

- implications for interpreting satellite-based SIF retrievals. *Remote Sens. Environ.* 205, 276–289.
- Zhao, M., Running, S.W., Nemani, R.R., 2006. Sensitivity of Moderate Resolution Imaging Spectroradiometer (MODIS) terrestrial primary production to the accuracy of meteorological reanalyses. *J. Geophys. Res.-Biogeosci.* 111.
- Zhao, M.S., Heinrich, F.A., Nemani, R.R., Running, S.W., 2005. Improvements of the MODIS terrestrial gross and net primary production global data set. *Remote Sens. Environ.* 95, 164–176.
- Zheng, Y., Shen, R.Q., Wang, Y.W., Li, X.Q., Liu, S.G., Liang, S.L., Chen, J.M., Ju, W.M., Zhang, L., Yuan, W.P., 2020. Improved estimate of global gross primary production for reproducing its long-term variation, 1982–2017. *Earth Syst. Sci. Data* 12, 2725–2746.
- Zheng, Y., Zhang, L., Xiao, J., Yuan, W., Yan, M., Li, T., Zhang, Z., 2018. Sources of uncertainty in gross primary productivity simulated by light use efficiency models: Model structure, parameters, input data, and spatial resolution. *Agric. For. Meteorol.* 263, 242–257.
- Zhu, H., Lin, A., Wang, L., Xia, Y., Zou, L., 2016. Evaluation of MODIS gross primary production across multiple biomes in China using eddy covariance flux data. *Remote Sens.* 8.
- Zhu, X., Pei, Y., Zheng, Z., Dong, J., Zhang, Y., Wang, J., Chen, L., Doughty, R.B., Zhang, G., Xiao, X., 2018. Underestimates of grassland gross primary production in MODIS standard products. *Remote Sens.* 10.